OPTOFLUIDIC APPROCHES IN RECONFIGURABLE PHOTONICS AND RENEWABLE ENERGY

A Dissertation

Presented to the Faculty of the Graduate School

of Cornell University

In Partial Fulfillment of the Requirements for the Degree of

Doctor of Philosophy

by

Eunjung Jung

August 2013

OPTOFLUIDIC APPROCHES IN RECONFIGURABLE PHOTONICS AND RENEWABLE ENERGY

Eunjung Jung, Ph. D.

Cornell University 2013

The theme of my Ph.D. research is to apply optofluidics to solve problems in interdisciplinary areas, specifically reconfigurable photonics and photobioreactors for microalgae based biofuel production. In the first part of the dissertation, I have developed a hybrid reconfigurable photonic system that combines liquid and solid state optical waveguides on a chip. The hybrid system was numerically and experimentally investigated. The apparatus allowed us to take advantages of liquid-state optical elements, such as chemical adaptability, thermal stabilization, and physical tunability, without sacrificing the performance offered by solid-state optical devices. This novel approach represents a potentially transformative advancement for reconfigurable photonic systems. In the second part of the dissertation, I have developed optofluidic photobioreactors that incorporate photonic elements to solve problems in current photobioreactors for algae biofuel production. I first demonstrated and characterized photosynthetic growth in the evanescent field of a slab waveguide. The bacterial growth has been further demonstrated in a 10 stack waveguide photobioreactor. This novel optofluidic photobioreactor increases the culture density that can result in cost-effective bioreactors with lower operational costs and reduced water and energy consumption.

BIOGRAPHICAL SKETCH

Eunjung (Erica) Jung was born in 1984 and grew up in Seoul, Korea. She completed her bachelor's degree in 2006 from the Department of Mechanical and Aerospace Engineering at Sungkyunkwan University. She earned her Master in Science in 2008 from the Department of Mechanical and Aerospace Engineering at Korea Advanced Institute of Science and Technology (KAIST). Eunjung then moved to the U.S. for her graduate studies and joined Erickson lab in Mechanical Engineering at Cornell University in 2008. During her study at Cornell University, she has been involved in projects, "Reconfigurable Materials for Cellular Electronic and Photonic Systems discovery challenge thrust" funded by Air force and "High Density Photobiorefineries with Optimized Light/CO2 Delivery and Product Extraction" funded by ARPA-e.

To my dear and loving husband, Frank

ACKNOWLEDGMENTS

First of all, I would like to thank Prof. Erickson, committee chair for my Ph.D. study. I can say that he is one of the greatest advisors who I have ever interacted with. His guidance and enthusiasm to research always motivated me to solve difficulties in my research. He has been my role model as a leader and a scientist. I am grateful to be a student under his guidance.

I would like to thank my committee members, Prof. Clifford Pollock and Prof. Antje Baeumner. I appreciate all of their support and thoughtful advices on my research and post graduate career planning as well. I also would like to thank all of my colleagues and alumni in Erickson lab. Especially I would like to thank Aram Chung who was a third year Ph.D. student when I joined in Erickson lab and now is a faculty member at Rensselaer Polytechnic Institute. Since the first day in Ithaca, he has been a great mentor throughout graduate studies in discussing both academic and non-academic topics. I wish all goes well for him at RPI. And I would like to thank my colleagues, Michael Kalontarov, Saad Ashan, Aadhar Jain, Devin Doud, Erik Bland, and Nina Voulis, who I have collaborated for the ARPA-e project. We were a great team and I could have not achieved anything without their supports. I also would like to thank my friends in Erickson lab notably Yun Suk Huh, Inhee Choi, Pilgyu Kang, Michael Mak, Xavier Serey, and Melaka Krishnan. It was always helpful to discuss with them when I encountered difficulties during my experiments.

Lastly and most importantly I would like to thank my family. First of all, my mom, she is an amazing person. She scarified her everything for my family and did not

forget her sense of humor in any difficult situations. She empowered me to overcome challenges and difficulties in my life. My dad, I know how much he loves me and cares our family. I truly appreciate everything that I have learned from my dad and his dedication to our family. I also would like to thank my sister, Jiyoun. She always yielded to me and shared a lot of hers with me. I hope everything is going well with her.

Finally, I would like to thank my husband, Frank. He is the greatest person who I have ever known. He is kind, generous, patient and admirable. I have never come to this point without him. He is my best friend and perfect partner in my life. Frank, I love you. I am the luckiest person in the world because I have you. And special thanks to our future baby. Dear baby, your mom and dad were extremely happy when we figured out you were there and now we are patiently waiting for you. You are a miracle that happened in my life. We love you more than you will ever know.

TABLE OF CONTENTS

LIST OF FIGURES

LIST OF SYMBOLS

v = velocity vector

ρ = fluid density

p = pressure

μ = viscosity

c = concentration

D = mass diffusion coefficient

V = average velocity

L = length scale

∇_t = the transverse part of ∇

E_t = the transverse electric field

k_0 = the free-space wavenumber

n_i = the refractive index of the medium

β = propagation constant

α = absorption coefficient

C= concentration of algae

d_p = penetration depth

I_0 = incident light

I = transmitted light

n_s = the refractive index of substrate

n_w = the refractive index of waveguide

n_c = the refractive index of cladding

γ_c = attenuation coefficient in the cladding

γ_c = attenuation coefficient in the substrate

k_w = the transverse component of k

θ_i = the angle of the incident light

θ_t = the angle of the refracted light

n_1 = the refractive index of the first medium

n_2 = the refractive index of the first medium

CHAPTER 1

INTRODUCTION

1.1 Optofluidics

Optofluidics refers to the fusion of fluidics with optics and photonics. Unique properties of fluids, such as physical adaptability over very large distances, widely tunable optical properties, and inherent convective processes that improve heat transfer and provide better thermal stabilization, can be utilized in the enhancement of solid state photonics. Solid state optical components, on the other hand, have demonstrated its superior abilities in providing advanced functionalities, such as signal modulations and active filtering, fast switching speed, and precise manipulation on small molecules. Combining these liquid and solid state components has brought synergetic effects in a number of areas including: plasmonic [1-3], biomedical sensing [4, 5], optical imaging [6, 7], optical manipulation [8, 9], adaptive lenses [10, 11], data storage [12], and energy applications [13]. While optofluidic techniques were successfully adapted in these areas, to date little work has been done to integrate liquid and solid state optical waveguides on the same platform and to address problems in photobioreactors for algae biofuel production. In the first part of this dissertation, chapter 2 and 3, I developed novel optofluidic techniques for reconfigurable photonics that enable the integration of two state optical waveguides on the same platform to leverage the advantages of both elements. In the second part of this dissertation,

chapter 4 and 5, I developed a new class of optofluidic photobioreactors that highly enhance the volumetric productivity for algae biofuel production.

1.2 Optofluidic applications in reconfigurable photonics and renewable energy

1.2.1 Optofluidics for reconfigurable photonics

Integration of microfluidic components to handle light in optical systems was one of the early concepts of optofluidics [13-17]. The concept has resulted in a number of technologies including: liquid-state optical lenses [18-21], dye lasers [22, 23], and liquid-core/liquid-cladding optical waveguides [24-27]. The latter of the optofluidic techniques has a number of significant advantages compared to conventional solid waveguides including: physical adaptability (*i.e.* the light path or mode profile can be reconfigured on command simply by adjusting the local flow conditions), chemical adaptability (*i.e.* varying levels of gain media or non-linear solutions can be introduced to or removed from the waveguide) and thermal stabilization. Despite these advantages, the complete replacement of traditional solid-state photonic elements with liquid-state ones is not achievable due their relatively low switching speed [28] and inability to perform advanced functionalities such as signal modulation [29, 30] or active filtering [31].

One approach that allows us to take the advantages of liquid and solid-state photonic waveguides is to combine the two state components into hybrid optofluidic systems. By combining liquid and planar solid state components on a chip, it is

possible to establish a new optical platform which is not only flexible and reconfigurable, but also fast, stable and easy to operate.

In chapter 2, I presented a microfluidically reconfigurable photonic system to combine liquid and solid state waveguides and a numerical method to analyze the hybrid system as a function of Peclet number of the liquid waveguide. I investigated both evanescent and end-fire coupling from the liquid to solid optical waveguide. In chapter 3, I experimentally demonstrated and characterized the conditions for direct coupling between liquid and solid waveguides on a silicon substrate. Tunable end-fire and evanescent coupling between the liquid- and solid-core waveguides were demonstrated for the first time. In addition, a novel fluidic recirculation system that eliminates the need for the resupply or removal of liquids was demonstrated by the use of immiscible liquids and on-chip separation columns.

1.2.2 Optofluidics for renewable energy

Algal biofuel is one of the most promising alternatives to solve current energy problems due to the high oil yields, fastest growth rate among plants and no competition with food crop for land. Despite these advantages, there are major challenges that prevent economically viable algal biofuel production. One major challenge is the non-uniform distribution of light within existing photobioreactors [32]. (*e.g.* open-to-air pond reactors or closed-systems tube reactors [33-35]). Due to the shading effect caused by dense microalgae cultures, the organisms near the reactor surface are easily overexposed and the organisms away from the surface [36] are

underexposed. The uneven distribution of light significantly reduces the volumetric productivities [37, 38].

Optofluidics can offer a solution to the challenge in algae-derived biofuel production [13]. Optofluidics has demonstrated its ability to simultaneously control light and fluid to study living organisms. For instance, optical tweezers provide us a unique tool to sort, trap and manipulate cells and DNAs [39-43] in an aqueous environment. Biosensors, such as optical resonators and planar waveguides utilizing an evanescent field to detect the difference in the refractive index [44-47], have been integrated with fluidic units to analyze biomolecular interactions. This synergetic effect of optical and fluidic controls over living organisms demonstrates potential applications of optofluidic techniques in constructing photobioreactors. At present however, only a limited number of the optofluidic techniques have been applied to address problems in algae biofuel production.

In chapter 4, I presented novel photobioreactors that adapted optofluidic approaches to enhance the volume productivity of current photobioreactors for microalgae based biofuel production. By incorporating slab waveguides to deliver light to photosynthetic organisms through the evanescent field, I have demonstrated here a new form of photobioreactors that improve the light distribution while being compatible with these fuel secreting organisms. In chapter 5, I presented stackable ultracompact photobioreactors. Advanced photonics, the demonstrated evanescent illumination and light scatterings on the surface of planar waveguides, have been applied to achieve an even distribution of light in stackable photobioreactors. The

bacterial growth and fuel production in a 10 stack waveguide photobioreactor has been demonstrated.

1.3 Theoretical background

1. 3.1 Light propagation in liquid core-liquid cladding waveguide

To obtain solutions of light propagation within an optical waveguide, refractive index (RI) profile has to be known. A liquid waveguide has a continuous distribution of RI due to the diffusion of the liquid core dopant into the cladding. To obtain the RI profile for the liquid waveguide, which is correlated to its concentration profile, the fluid dynamical continuity and conservation of momentum equations in steady state, Eq. (1.1a) and (1.1b), must first be solved to obtain the velocity field. Once the velocity field is obtained we can solve the steady state convection-diffusion equation, Eq. (1.2), to obtain the concentration profile *c*. With the concentration profile, the RI profile can be obtained directly from experimental data that measures refractive indices at different concentrations.

$$\nabla \cdot \mathbf{v} = 0 \qquad (1.1a)$$

$$\rho \mathbf{v} \cdot \nabla \mathbf{v} = -\nabla p + \mu \cdot \nabla^2 \mathbf{v} \qquad (1.1b)$$

$$\mathbf{v} \cdot \nabla c = D \nabla^2 c \qquad (1.2)$$

In Eq. (1.1a) and (1.1b) **v**, ρ, p, and μ are velocity vector, fluid density, pressure and viscosity respectively. In Eq. (1.2) c and D are the concentration and the mass

diffusion coefficient. We can nondimensionalize Eq (1.1b) and (1.2) to (1.3) and (1.4) by considering reference parameters V and L, average velocity and length scale. The Reynolds number in Eq. (1.3), $Re = \rho VL / \mu$, is a ratio of inertial forces to viscous forces. In micro scale flows, the left hand side of the Eq. (1.3) can be ignored and two dominant parameters, the pressure and viscosity, cause laminar flow. The Peclet number in Eq. (1.4), $Pe = VL / D$, is a ratio of convective transport to diffusive transport. The increase of Peclet number means that diffusive mixing of fluids in the channel is reduced. In Eq. (1.3) and (1.4), nondimensional variables are denoted by starred properties: $\mathbf{v}^* = \mathbf{v}/V$, $p^* = \mu V / L$, $\nabla^* = \nabla \cdot L$, $\nabla^{*2} = \nabla \cdot L^2$.

$$Re \cdot (\mathbf{v}^* \cdot \nabla^* \mathbf{v}^*) = -\nabla^* p^* + \nabla^{*2} \mathbf{v}^* \qquad (1.3)$$

$$Pe \cdot (\mathbf{v}^* \cdot \nabla^* c) = \nabla^{*2} c \qquad (1.4)$$

With the refractive index profile obtained from the convection-diffusion equations above, the wave equation can be solved to obtain solutions of light propagation within the waveguide. Under the assumption of the negligibly small gradient in the permittivity of the medium, the wave equation can be expressed as

$$\nabla_t^2 E_t + (k_0^2 n_i^2 - \beta^2) E_t = 0 \qquad (1.5)$$

where ∇_t, E_t, k_0, n_i and β are the transverse part of ∇, the transverse electric field, the free-space wavenumber, the refractive index of the medium and the propagation constant respectively. In a case where the liquid waveguide is confined within a microchannel or near a surface, obtaining analytical solution is not possible and therefore numerical techniques must be used.

1.3.2 Light penetration depth in photobioreactors (PBRs) and photoinhibition of photosystem II (PSII)

The light penetration depth in photobioreactors can be calculated by Beer lambart's law.

$$e^{-\alpha C d_p} = \frac{I}{I_0} \qquad (1.6)$$

Where α, C, d_p are the absorption coefficient, concentration of organism and penetration depth. I_0 and I and incident and transmitted light respectively. According to the equation, the light penetration depth in photobioreactors is determined by the absorption coefficient and concentration of organism in reactors. For green algae, the relation between the penetration depth and the concentration of algae can be simplified by the equation proposed by Oswald in 1988 [48].

$$d_p = 6000/C \qquad (1.7)$$

Where d_p and C are the penetration depth (cm) and concentration of algae (mg· L^{-1}). Due to the exponential decrease of light intensity in photobioreactors, algae on the surface of the reactor can be overexposed and photoinhibited while ones deep inside the photobioreactor are exposed to insufficient light for growth or none of the light. The uneven distribution of light in photobioreactors becomes more serious when the concentration of algae increases. This phenomenon has been a major challenge in current photobioreactors to achieve a high volumetric productivity.

Photoinhibition of photosystem II (PSII) occurs when the system is exposed under strong light that causes imbalance between the rate of photodamage to PSII and the rate of the repair of damaged PSII [49]. For cyanobacteria, photon flux over 150 μE ~ 500 μE can cause the photoinhibition of PSII [50].

1.3.3 Evanescent field and light scattering generated on the surface of optical waveguides

To overcome the uneven distribution of light in photobioreactors that has been described in the 1.3.2, optical approaches, an evanescent field and light scatterings generated on the surface of waveguides, were employed in my research. The evanescent field is a near field that exponentially decays from the dielectric interface of an optical waveguide. When the longitudinal wave vector (β) satisfy the condition that $k_0 n_s < \beta < k_0 n_w$, where k_0, n_s and n_w are the free-space wavenumber, the refractive index of a substrate and a waveguide respectively and where it is assumed that $n_c \leq n_s$ where n_c is the refractive index of a cladding, light is totally reflected back from the both side of the waveguide(Fig. 1.1). The guided light in the waveguide generates the evanescent field at the dielectric interface.

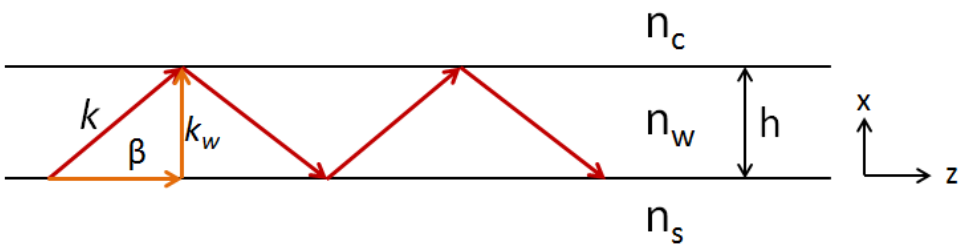

Figure 1.1 Guided light in an optical waveguide with refractive index of n_w.

When the E field is polarized along the y axis and propagating along the z axis in Fig. 1.1 (TE mode), solutions of Eq. (1.5) can be obtained applying boundary conditions that TE and TH are continuous at the interfaces [51]. The solutions are

$$E_y(x) = Ae^{-\gamma_c x} \qquad x > 0 \qquad (1.8)$$

$$E_y(x) = A\left[\cos(k_w x) - \frac{\gamma_c}{k_w}\sin(k_w x)\right] \qquad -h < x < 0 \qquad (1.9)$$

$$E_y(x) = A\left[\cos(k_w x) + \frac{\gamma_c}{k_w}\sin(k_w x)\right] e^{\gamma_s (x+h)} \qquad x < -h \qquad (1.10)$$

Where A is the amplitude at the $x = 0$. γ_c and γ_s are attenuation coefficients in the cladding and substrate respectively. k_w is the transverse component of k in the waveguide. As shown in the solutions, the evanescent field (where x > 0 and x < -h) exponentially decays from the surface of the waveguide.

Another light source from the waveguide that photosynthetic bacteria can utilize is scattered lights. When lights hit scatters on the surface of the waveguide with angles smaller than a critical angle, part of lights reflect and the rest of lights transmit at the interface as shown in Fig. 1.2.

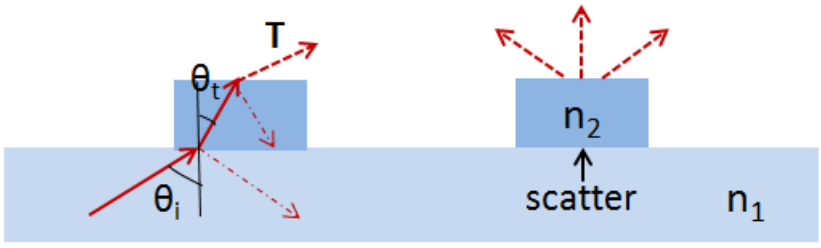

Figure 1.2. Light scatterings at scatters on the surface of the waveguide

The transmission angle is governed by Snell's law.

$$\frac{\sin\theta_i}{\sin\theta_t} = \frac{n_2}{n_1} \qquad (1.11)$$

Where θ_i and θ_t are the angle of incident and transmitted lights. n_1 and n_2 are the refractive index of the first and second medium. The fractions that are reflected and transmitted are given by the reflection coefficient *R* and the transmittance coefficient *T* respectively. When the incident light is a TE mode, the reflection and transmittance coefficients, *R* and *T* are expressed as below according to the Fresnel equations.

$$R = \left|\frac{n_1\cos\theta_i - n_2\cos\theta_t}{n_1\cos\theta_i + n_2\cos\theta_t}\right|^2 \qquad (1.12)$$

$$T = 1 - R \qquad (1.13)$$

The scatters can be precisely engineered to achieve the uniform distribution of light along the waveguide.

1.4 Research Overview and Dissertation Breakdown

Chapter 2 presents a comprehensive analytical and numerical study of the use of liquid state elements in reconfigurable photonics. I developed a new approach to reconfigurable photonics which allows us to take advantage of the chemical and physical adaptability of liquid state photonics with the robustness and speed available from traditional solid state photonics As I discussed in details in the chapter 2, since

both the solid and liquid state elements are reasonably well developed, the major challenge in realizing this platform is in the development of technique that allows one to transfer light from the liquid state to the solid state and back again. By combining liquid and planar solid state components on a chip, it is possible to establish a new optical platform which is not only flexible and reconfigurable, but also fast, stable and easy to operate. The importance of this study is that I performed the first electro-hydro-dynamic study of these liquid state optical systems as a function of relevant microfluidic transport parameters such as the Peclet number. In the first part of this work I examined purely liquid state phenomena such as mode field diameter and bending loss and investigated both evanescent and end-fire liquid-to-solid optical coupling schemes. In the second part of this work, uniquely fluid-optical effects were demonstrated including irreversible evanescent coupling and dynamic mode field matching.

Chapter 3 shows the experimental demonstration of the liquid-solid state reconfigurable photonic system. As I discussed in chapter 2, there are a number of truly fundamental advantages that the incorporation of liquid state elements into reconfigurable photonic systems could offer. At present however this fusion is not practical due to the inability to transfer light from liquid state waveguides to on-chip solid state elements and the need to continuously re-supply liquids. By developing unique solid-to-liquid-to-solid state coupling techniques and on-chip gravity based liquid core/cladding separation system and I have demonstrated here the ability to address both these major roadblocks. Quantitatively I demonstrated the ability to reduce liquid consumption over 1,000-fold compared to the state of the art, while

enabling reconfiguration on the order of 100 times greater than what is achievable with other optomechanical approaches.

In chapter 4, a novel optofluidic photobioreactor that can help address two major challenges in algae derived biofuel production is introduced. Put simply, microalgae based biofuel production has a number of advantages over land based feed stocks. At present however commercially viable microalgae-derived biofuel production is complicated by the non-uniform distribution of light within current photobioreactors that results in a poor volumetric productivity and the high cost associated with traditional biomass processing (e.g. harvesting and oil extraction from microalgae). The latter problem can be addressed by genetically modified photosynthetic organisms that directly secrete chemical precursors to fuels without requiring the biomass processing. By incorporating slab waveguides to deliver light to photosynthetic organisms through the evanescent field, I have demonstrated here a new form of stackable photobioreactor that improves the light distribution while being compatible with these fuel secreting organisms. For the first time, I have demonstrated and characterized the growth of photosynthetic organisms using the evanescent field on a slab waveguide.

Chapter 5 presents a stackable ultracompact photobioreactor that highly improves the volumetric productivity of photobioreactors for the algae biofuel production. The stackable layout demonstrated in chapter 4 has been examined in a 10 stack waveguide photobioreactor. I have applied optofluidic approaches, the evanescent illumination and light scatterings on the surface of planar waveguides, to achieve an even

distribution of light in the photobioreactors. The growth of fuel producing bacteria and the fuel production in the 10 stack photobioreactor have been demonstrated and characterized.

Chapter 6 summarizes my research contributions in reconfigurable photonics and photobioreactors for biofuel production based on microalgae.

REFERENCES

1. Choi, Y., et al., *Selective and sensitive detection of metal ions by plasmonic resonance energy transfer-based nanospectroscopy.* Nature Nanotechnology, 2009. **4**(11): p. 742-746.
2. Cho, H.S., et al., *Single-Step Nanoplasmonic VEGF(165) Aptasensor for Early Cancer Diagnosis.* Acs Nano, 2012. **6**(9): p. 7607-7614.
3. Stewart, M.E., et al., *Nanostructured plasmonic sensors.* Chemical Reviews, 2008. **108**(2): p. 494-521.
4. Mandal, S. and D. Erickson, *Nanoscale optofluidic sensor arrays.* Optics Express, 2008. **16**(3): p. 1623-1631.
5. Zhu, H.Y., et al., *Analysis of biomolecule detection with optofluidic ring resonator sensors.* Optics Express, 2007. **15**(15): p. 9139-9146.
6. Cui, X.Q., et al., *Lensless high-resolution on-chip optofluidic microscopes for Caenorhabditis elegans and cell imaging.* Proceedings of the National Academy of Sciences of the United States of America, 2008. **105**(31): p. 10670-10675.
7. Heng, X., et al., *Optofluidic microscopy - a method for implementing a high resolution optical microscope on a chip.* Lab on a Chip, 2006. **6**(10): p. 1274-1276.
8. Chen, Y.F., et al., *Controlled Photonic Manipulation of Proteins and Other Nanomaterials.* Nano Letters, 2012. **12**(3): p. 1633-1637.

9. Kang, P., et al., *Angular Orientation of Nanorods Using Nanophotonic Tweezers.* Nano Letters, 2012. **12**(12): p. 6400-6407.

10. Nguyen, N.T., *Micro-optofluidic Lenses: A review*. Biomicrofluidics, 2010. **4**(3).

11. Song, C.L., et al., *Tunable micro-optofluidic prism based on liquid-core liquid-cladding configuration.* Optics Letters, 2010. **35**(3): p. 327-329.

12. Cordovez, B., D. Psaltis, and D. Erickson, *Electroactive micro and nanowells for optofluidic storage.* Optics Express, 2009. **17**(23): p. 21134-21148.

13. Erickson, D., D. Sinton, and D. Psaltis, *Optofluidics for energy applications.* Nature Photonics, 2011. **5**(10): p. 583-590.

14. Psaltis, D., S.R. Quake, and C.H. Yang, *Developing optofluidic technology through the fusion of microfluidics and optics.* Nature, 2006. **442**(7101): p. 381-386.

15. Monat, C., P. Domachuk, and B.J. Eggleton, *Integrated optofluidics: A new river of light.* Nature Photonics, 2007. **1**(2): p. 106-114.

16. Schmidt, H. and A.R. Hawkins, *The photonic integration of non-solid media using optofluidics.* Nature Photonics, 2011. **5**(10): p. 598-604.

17. Fan, X.D. and I.M. White, *Optofluidic microsystems for chemical and biological analysis.* Nature Photonics, 2011. **5**(10): p. 591-597.

18. Krupenkin, T., S. Yang, and P. Mach, *Tunable liquid microlens.* Applied Physics Letters, 2003. **82**(3): p. 316-318.

19. Pang, L., et al., *Set of two orthogonal adaptive cylindrical lenses in a monolith elastomer device.* Optics Express, 2005. **13**(22): p. 9003-9013.

20. Mao, X.L., et al., *Hydrodynamically tunable optofluidic cylindrical microlens.* Lab on a Chip, 2007. **7**(10): p. 1303-1308.

21. Tang, S.K.Y., C.A. Stan, and G.M. Whitesides, *Dynamically reconfigurable liquid-core liquid-cladding lens in a microfluidic channel.* Lab on a Chip, 2008. **8**(3): p. 395-401.

22. Li, Z.Y., et al., *Single mode optofluidic distributed feedback dye laser.* Optics Express, 2006. **14**(2): p. 696-701.

23. Song, W.Z. and D. Psaltis, *Pneumatically tunable optofluidic dye laser.* Applied Physics Letters, 2010. **96**(8).

24. Wolfe, D.B., et al., *Dynamic control of liquid-core/liquid-cladding optical waveguides.* Proceedings of the National Academy of Sciences of the United States of America, 2004. **101**(34): p. 12434-12438.

25. Seow, Y.C., S.P. Lim, and H.P. Lee, *Tunable optofluidic switch via hydrodynamic control of laminar flow rate.* Applied Physics Letters, 2009. **95**(11).

26. Lee, K.S., et al., *Three-dimensional microfluidic liquid-core/liquid-cladding waveguide.* Applied Physics Letters, 2010. **97**(2).

27. Yang, Y., et al., *A tunable 3D optofluidic waveguide dye laser via two centrifugal Dean flow streams.* Lab on a Chip, 2011. **11**(18): p. 3182-3187.

28. Hache, A. and M. Bourgeois, *Ultrafast all-optical switching in a silicon-based photonic crystal.* Applied Physics Letters, 2000. **77**(25): p. 4089-4091.

29. Xu, Q.F., et al., *Micrometre-scale silicon electro-optic modulator.* Nature, 2005. **435**(7040): p. 325-327.

30. Levy, J.S., et al., *CMOS-compatible multiple-wavelength oscillator for on-chip optical interconnects.* Nature Photonics, 2010. **4**(1): p. 37-40.

31. Park, H.G., et al., *A wavelength-selective photonic-crystal waveguide coupled to a nanowire light source.* Nature Photonics, 2008. **2**(10): p. 622-626.

32. Grima, E.M., et al., *Photobioreactors: light regime, mass transfer, and scaleup.* Journal of Biotechnology, 1999. **70**(1-3): p. 231-247.

33. Janssen, M., et al., *Enclosed outdoor photobioreactors: Light regime, photosynthetic efficiency, scale-up, and future prospects.* Biotechnology and Bioengineering, 2003. **81**(2): p. 193-210.

34. Posten, C., *Design principles of photo-bioreactors for cultivation of microalgae.* Engineering in Life Sciences, 2009. **9**(3): p. 165-177.

35. Lehr, F. and C. Posten, *Closed photo-bioreactors as tools for biofuel production.* Current Opinion in Biotechnology, 2009. **20**(3): p. 280-285.

36. Lee, C.-G., *Calculation of light penetration depth in photobioreactors.* Biotechnology and Bioprocess Engineering, 1999. **4**(1): p. 78-81.

37. Bosma, R., et al., *Prediction of volumetric productivity of an outdoor photobioreactor.* Biotechnology and Bioengineering, 2007. **97**(5): p. 1108-1120.

38. Grima, E.M., et al., *A study on simultaneous photolimitation and photoinhibition in dense microalgal cultures taking into account incident and averaged irradiances.* Journal of Biotechnology, 1996. **45**(1): p. 59-69.

39. Grier, D.G., *A revolution in optical manipulation.* Nature, 2003. **424**(6950): p. 810-816.

40. Svoboda, K. and S.M. Block, *BIOLOGICAL APPLICATIONS OF OPTICAL FORCES.* Annual Review of Biophysics and Biomolecular Structure, 1994. **23**: p. 247-285.

41. Ashkin, A., *Optical trapping and manipulation of neutral particles using lasers.* Proceedings of the National Academy of Sciences of the United States of America, 1997. **94**(10): p. 4853-4860.

42. Chen, Y.-F., et al., *Controlled photonic manipulation of proteins and other nanomaterials.* Nano Letters, 2012. **12**(3): p. 1633-7.

43. Mandal, S., X. Serey, and D. Erickson, *Nanomanipulation Using Silicon Photonic Crystal Resonators.* Nano Letters, 2010. **10**(1): p. 99-104.

44. Mandal, S., J.M. Goddard, and D. Erickson, *A multiplexed optofluidic biomolecular sensor for low mass detection.* Lab on a Chip, 2009. **9**(20): p. 2924-2932.

45. Mancuso, M., J.M. Goddard, and D. Erickson, *Nanoporous polymer ring resonators for biosensing.* Optics Express, 2012. **20**(1): p. 245-255.

46. Cooper, M.A., *Label-free screening of bio-molecular interactions.* Analytical and Bioanalytical Chemistry, 2003. **377**(5): p. 834-842.

47. Fan, X.D., et al., *Sensitive optical biosensors for unlabeled targets: A review.* Analytica Chimica Acta, 2008. **620**(1-2): p. 8-26.

48. Oswald, W.J., *MICRO-ALGAE AND WASTE-WATER TREATMENT*. Borowitzka, M. A. And L. J. Borowitzka1988. 305-328.

49. Murata, N., et al., *Photoinhibition of photosystem II under environmental stress.* Biochimica Et Biophysica Acta-Bioenergetics, 2007. **1767**(6): p. 414-421.

50. Kulkarni, R.D. and S.S. Golden, *ADAPTATION TO HIGH LIGHT-INTENSITY IN SYNECHOCOCCUS SP STRAIN PCC-7942 - REGULATION OF 3 PSBA GENES AND 2 FORMS OF THE D1 PROTEIN.* Journal of Bacteriology, 1994. **176**(4): p. 959-965.

51. Pollock, C.R., *Fundamentals of Optoelectronics*1994: Richard D Irwin.

CHAPTER 2

ANALYSIS OF LIQUID-TO-SOLID COUPLING AND OTHER PERFORMANCE PARAMETERS FOR MICROFLUIDICALLY RECONFIGURABLE PHOTONIC SYSTEMS

2.1 Abstract

In this paper, we analytically investigate the coupling of light from liquid-core waveguides to conventional solid-core waveguides and a series of other optical properties of liquid waveguides in order to gauge the practicality of such a system for use in microfluidically reconfigurable photonic systems. A finite element model of the system was constructed and relevant properties such as mode field diameter, attenuation, bending loss, and efficiency of evanescent and end-fire coupling were investigated as a function of the liquid waveguide Peclet number and the relative difference in refractive index. For pure liquid systems we show that the mode field diameter decreases monotonically with increasing Peclet number and that bending losses could be significantly reduced by increasing the Peclet number. More critically, we observed irreversible evanescent coupling, in which the light coupled in the solid waveguide is entrapped within the solid rather than coupled back into the liquid waveguide. This effect was caused by the lengthwise variation in the propagation constant of the liquid core due to downstream diffusion. We demonstrate that coupling efficiencies as high as 84% can be obtained for fluid based end-fire coupling by taking advantage of the tunable mode field diameter. By developing techniques for coupling

light between liquid and solid states we hope to be able to overcome the drawbacks of solid waveguide systems (e.g. unchangeable structure and properties) and liquid waveguide systems (e.g. diversion and attenuation) yielding a new paradigm for reconfigurable photonics.

2.2 Introduction

Since its inception, Optofluidics[1,2], or the fusion of microfluidics with optics, has had significant impact in a number of areas including: optical biosensors, lensing and imaging[3-5], nanomanipulation[6-7], and on-chip waveguiding and lasing[8,9]. A popular approach to the latter of these is through the use of liquid core/fluid cladding waveguides[10-12] which represent a new type of optical element whereby a high refractive index liquid is cladded by a lower refractive index fluid are used to guide light around on a microfluidic chip. Compared to conventional solid waveguides, liquid waveguides have a number of significant advantages including: physical adaptability (*i.e.* the light path or mode profile can be reconfigured on command simply by adjusting the local flow conditions), chemical adaptability (*i.e.* varying levels of gain media or non-linear solutions can be introduced to or removed from the waveguide) and thermal stabilization. Despite these advantages, liquid state optical components are not likely to ever completely replace solid state optical components due to limitations in switching speed, general robustness and lack of advanced functionality such as active filtering or electro-optic modulation[13,14].

Recently we have proposed a new approach to reconfigurable photonics which allows us to take advantage of the chemical and physical adaptability of liquid state photonics with the robustness and speed available from traditional solid state photonics[15]. By combining liquid and planar solid state components on a chip, it is possible to establish a new optical platform which is not only flexible and reconfigurable, but also fast, stable and easy to operate. As we discuss in further detail below, since both the solid and liquid state elements are reasonably well developed,

the major challenge in realizing this platform is in the development of technique that allows one to transfer light from the liquid state to the solid state and back again. While numerous experimental studies of liquid waveguides have been performed[8-12], to date little theoretical work has been done to characterize the performance parameters of these devices, particularly related to liquid-solid coupling.

In this paper, we present a comprehensive analytical and numerical study of the use of liquid state elements in reconfigurable photonics. In the first part of the paper we use a coupled hydrodynamic-electromagnetic finite element model (FEM) to analyze liquid state behavior as a function of waveguide Peclet number, including mode field diameter and bending loss. The second part of the paper focuses on investigating both evanescent and end-fire liquid-to-solid optical coupling schemes. In addition to characterizing the coupling efficiency and length as a function of waveguide Pectlet number, uniquely fluid-optical effects are demonstrated including irreversible evanescent coupling and dynamic mode field matching.

2.3 Theory

To obtain the refractive index (RI) profile in the liquid waveguide, we first have to determine the flow velocity field and concentration profile of the solution dopant used to create the waveguide core. Once the RI profile is known the wave equation can be used to model the light propagation along the waveguide. In this section we provide details of the numerical method used to simulate the system.

2.3.1 Diffusion of liquid core in liquid waveguide

Instead of the step change in RI between the core and cladding as in a solid core waveguide, a liquid waveguide has a continuous distribution of RI which is caused by diffusion of the liquid core dopant into the cladding. The direction of the diffusion occurs both perpendicular to the direction of optical propagation, as with a conventional graded index waveguides, as well as parallel with it. To obtain the RI profile the fluid dynamical continuity and conservation of momentum equations in steady state, Eq. (2.1a) and (2.1b), must first be solved to obtain the velocity field. Once the velocity field is obtained it can be used as an input into the steady state convection-diffusion equation, Eq. (2.2), to obtain the concentration profile *c*. Once the concentration profile is obtained, the RI profile can be obtained directly from experimentally obtained values (solutions of calcium chloride, $CaCl_2$, were used in this study which ranges in refractive index from deionized water (n = 1.33) to 5M (n = 1.44)[16]).

$$\nabla \cdot \mathbf{v} = 0 \tag{2.1a}$$

$$\rho \mathbf{v} \cdot \nabla \mathbf{v} = -\nabla p + \mu \cdot \nabla^2 \mathbf{v} \tag{2.1b}$$

$$\mathbf{v} \cdot \nabla c = D \nabla^2 c \tag{2.2}$$

In Eq. (2.1a) and (2.1b) **v**, ρ, p, and μ are velocity vector, fluid density, pressure and viscosity respectively. In Eq. (2.2), c and D are the concentration and the mass diffusion coefficient. We can nondimensionalize Eq. (2.1b) and (2.2) by considering reference parameters V and L, average velocity and length scale. In Eq. (2.3a) and

(2.4a), nondimensional variables are denoted by starred properties: $\mathbf{v}^* = \mathbf{v}/V$, $p^* = \mu V / L$, $\nabla^* = \nabla \cdot L$, $\nabla^{*2} = \nabla \cdot L^2$.

$$Re \cdot (\mathbf{v}^* \cdot \nabla^* \mathbf{v}^*) = -\nabla^* p^* + \nabla^{*2} \mathbf{v}^* \quad (2.3a)$$

$$Re = \rho V L / \mu \quad (2.3b)$$

$$Pe \cdot (\mathbf{v}^* \cdot \nabla^* c) = \nabla^{*2} c \quad (2.4a)$$

$$Pe = VL / D \quad (2.4b)$$

Where *Re* and *Pe* are the Reynolds number and Peclet number respectively. The Reynolds number, Eq. (2.3b), is a ratio of inertial forces to viscous forces. In micro scale flows, the left hand side of the Eq. (2.3a) can be ignored and two dominant parameters, the pressure and viscosity, cause laminar flow (*Re* used in this paper was in the range of 0.1 ~1). The Peclet number, Eq. (2.4b), is a ratio of convective transport to diffusive transport. The increase of Peclet number means that diffusive mixing of fluids in the channel is reduced. Thus liquid waveguides with higher Peclet numbers would be expected to experience less downstream broadening.

2.3.2 Light propagation in liquid waveguide

Once the refractive index profile is obtained, the wave equation can be solved to obtain solutions of light propagation within the waveguide. Under the assumption of the negligibly small gradient in the permittivity of the medium, the wave equation can be expressed as

$$\nabla_t^2 E_t + (k_0^2 n_i^2 - \beta^2) E_t = 0 \quad (2.5)$$

where ∇_t, E_t, $k_{0,}$ n_i and β are the transverse part of ∇, the transverse electric field, the free-space wavenumber, the refractive index of the medium and the propagation constant respectively. Previous studies of conventional graded index waveguides [17] had rigid solid boundaries and diffusion layers only in the direction perpendicular to propagation. As alluded to above, in the case of liquid waveguide however the refractive index profile also changes along the direction of optical propagation. In the case where the flow is unconfined into a free solution it may be possible to obtain an analytical solution to the above set of equations. For the more generally applicable case where the waveguide is confined within a microchannel or near a surface such a solution is not possible and numerical techniques must be used.

2.3.3 Numerical method and boundary conditions

We performed detailed numerical simulations of light propagation in liquid waveguides and optical coupling from the liquid to the solid waveguide using a commercial finite element code. Figure 2.1 is a schematic of the elements of the liquid waveguide system we modeled here. Fluid flow was introduced by the pressure gradient between inlets, (1) and (2) in Fig. 2.1, and the outlet. Incompressible flow, constant viscosity and no slip boundary conditions at solid walls were assumed to compute the flow field. As mentioned above, we used solution of $CaCl_2$ (5M, n = 1.44) as the core solution. In all cases the core was focused into the microchannel between two cladding streams of DI water (n = 1.33) under the assumption of no reaction in the channel. Once we obtain the concentration profile, the transverse

electric (TE) mode polarized along the Z-direction was excited at the inlet of the core stream. The output boundary of the liquid waveguide was terminated by a perfectly matched layer. The simulations of the flow, concentration and electromagnetic fields were decoupled; thus each of the simulations was solved independently in the sequence of the flow field, concentration field and electromagnetic field.

As has been previously demonstrated [8], the cladding liquids with low RI sandwich the core liquid with high RI to obtain total internal refraction of the light within the liquid waveguide. Liquid waveguides were designed to be 1.5 μm wide at the inlet in order to support only the fundamental TE mode at a working wavelength of 1550 nm. Total length of the microchannel used in the paper is 500μm and the width is 20μm. Peclet numbers analyzed in this paper are in the range from 100 to 1000 and flow rates corresponding to the Peclet numbers are in the range from 0.005m/s to 0.05m/s. All simulations done in this paper are done using a 2D computational domain, which we believe is sufficient to capture the essential physics of the waveguide characterization and coupling parameters of interest here. Out of plane influences such as: the additional diffusive transport of the waveguide core, the 3D shape the liquid waveguide would assume as it interacted with a ridge waveguide, and the more complex velocity patterns which result from the presence of an upper and lower surfaces (in particular the generation of Dean's vorticies for curved channels at high flow velocities) would not be fully captured by our model. The latter of these limitations is discussed in more detail in section 3.2.

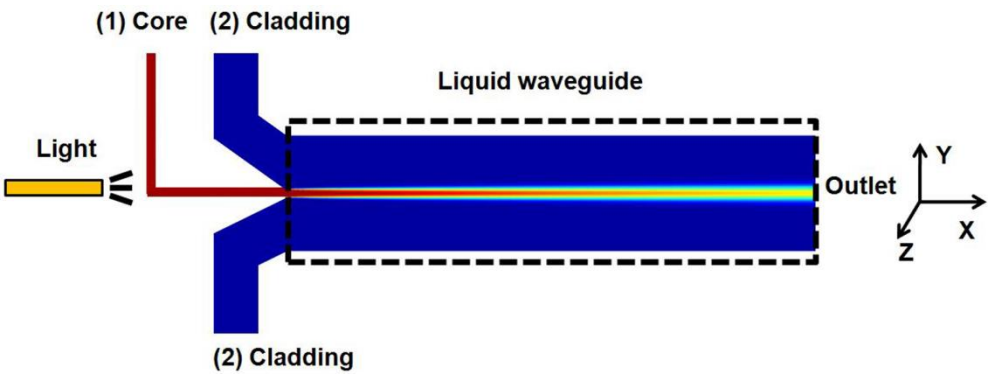

Figure 2.1 Schematic diagram of the liquid waveguide. Dotted area was simulated in this paper

2.4 Results and discussion: light propagation in liquid waveguide

As described in detail in section 2.1, the diffusive behavior of the waveguide (and consequently its local refractive index profile) is governed by the magnitude of the transport Peclet number. By extension then, it is reasonable to expect that both the optical performance and waveguide characteristics will both be strongly dependent on the Peclet number. As a result, prior to beginning our detailed analysis of the coupling between liquid and solid core systems, we will examine in detail how relevant optical properties such as mode field diameter (MFD), attenuation, and bending loss are dependent on it.

2.4.1 Mode field diameter and attenuation

For the case of interest here the Mode Field Diameter (MFD) [18] is representative of how tightly light is confined within the waveguide. Generally speaking the lower the

index contrast between the core and the cladding of the waveguide, the larger the MFD. In the case of the liquid waveguide, the contrast of the refractive indices of the core liquid and cladding liquid becomes lower as the core liquid diffuses as it is transported downstream resulting in an ever increasing MFD along the length of the waveguide. The effect is illustrated in Fig. 2.2(a) and 2.2.(b), which shows the refractive index and the steady state electric field profiles at *Pe* = 200, and Fig. 2.2(c) and 2.2(d), which shows the refractive index and the steady state electric field profiles at *Pe* = 800. Figure 2.2(e) and 2.2(f) show the power intensity distribution at the distance 300μm apart from the inlet, *Pe* = 200 and 800 respectively.

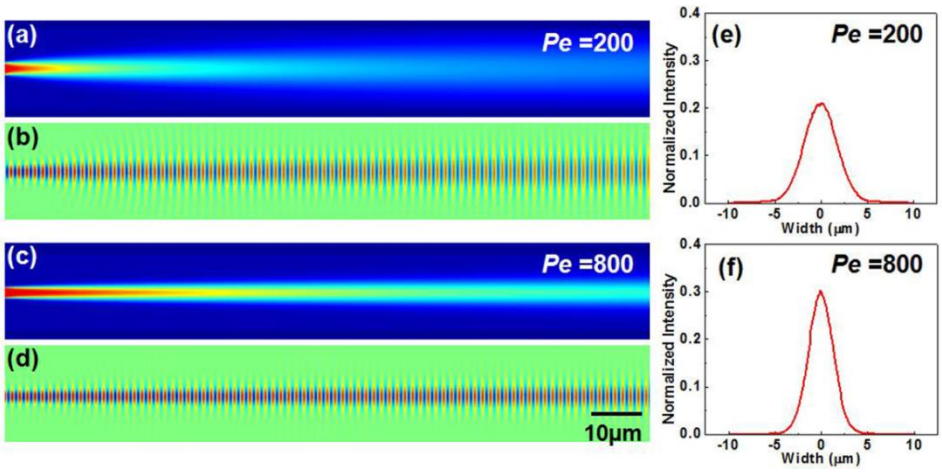

Figure 2.2 (a, b) Refractive index and steady state electric field profiles at *Pe* = 200. (c, d) Refractive index and steady state electric field profiles at *Pe* = 800. (e, f) Power intensity distribution at a downstream distance of 300μm, *Pe* = 200 and 800 respectively.

Figure 2.3(a) plots the MFD along the liquid waveguide at different Peclet numbers. MFD was estimated at the point that intensity dropped to $1/e^2$ of its maximum. As shown below, higher Peclet number resulted in a less dilute liquid core, and therefore a smaller mode field diameter (*e.g.* MFD at *Pe* = 800 was 6 μm while

MFD at *Pe* = 200 was 8.4 μm at the same downstream distance 500 μm). Diffusion of the liquid core resulted in not only broadening of MFD but also the attenuation of the optical power. Figure 2.3(b) shows that the liquid waveguide at *Pe* = 800 experienced a 0.14 dB attenuation while the liquid waveguide at *Pe* = 200 experienced a 1.06 dB attenuation at the same downstream distance 500 μm.

The change of MFD and the computed attenuation limit the distance over which the optical energy can be carried in the liquid element which is, of course, of primary concern in long distance communication applications. Although these effects may be reduced by using immiscible liquids, complete replacement of solid state optical components solely with liquid waveguides is likely not practical as current commercial optical fibers having attenuation values on the order of 10dB/km. Thus the integration of the liquid and solid elements is crucial to realize a fluidically reconfigurable photonic chip.

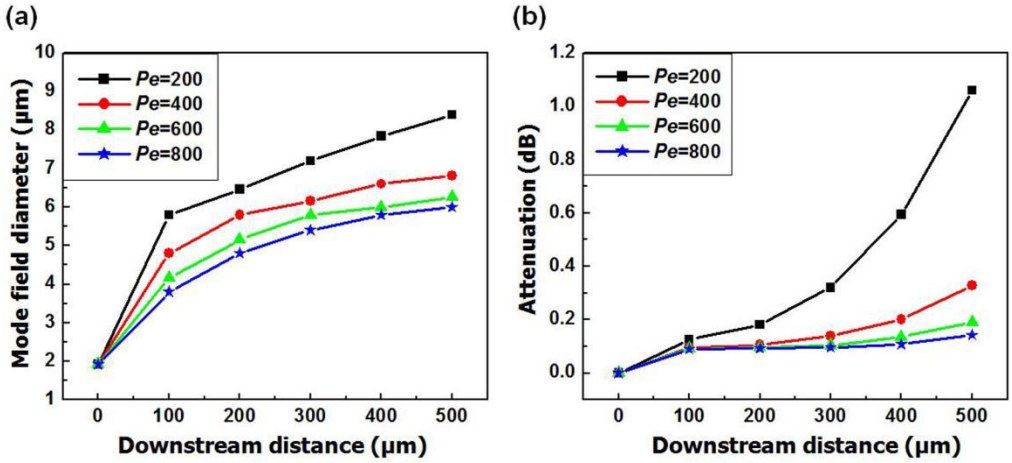

Figure 2.3 (a) Mode field diameter at different Peclet numbers along the liquid waveguide. (b) Attenuation of optical power at different Peclet numbers along the liquid waveguide

2.4.2 Bending loss

In traditional solid core waveguides bends tighter than the critical radius can result in significant loss of optical power[19,20]. Although it has yet to be characterized, we expect similar behavior in liquid core waveguides. An additional dependence on Peclet number is also expected, analogous to the above. We note that for the simulations conducted here, the Dean number for the ranges from $1.4x10^{-2}$ to $2.23x10^{-1}$ and thus below the conditions where one would expect to observe Dean vorticies in a fully 3D system. We therefore believe that our 2D model is valid for the conditions of interest here, however deviations from these trends are likely to be observed at much higher Pe numbers.

To characterize this we performed a series of simulations for the same liquid core system described above around a series of curved microchannels as shown in Fig. 2.4(a). To maintain consistency between each of the systems we made total length of the channels in each case the same distance, S_0 = 500 μm. Figure 2.4(b) shows the bending loss (dB) for different bending radii as a function of Peclet number. Similar to the bending loss in conventional solid waveguides, small bending radius decreased the power delivered through the bend. Higher Peclet numbers tended to reduce the bending loss due to its ability to confine the light more tightly (as described in section 3.1) and even in some cases a small radius bending with high Peclet number experienced less power loss than a large radius bending with low Peclet number.

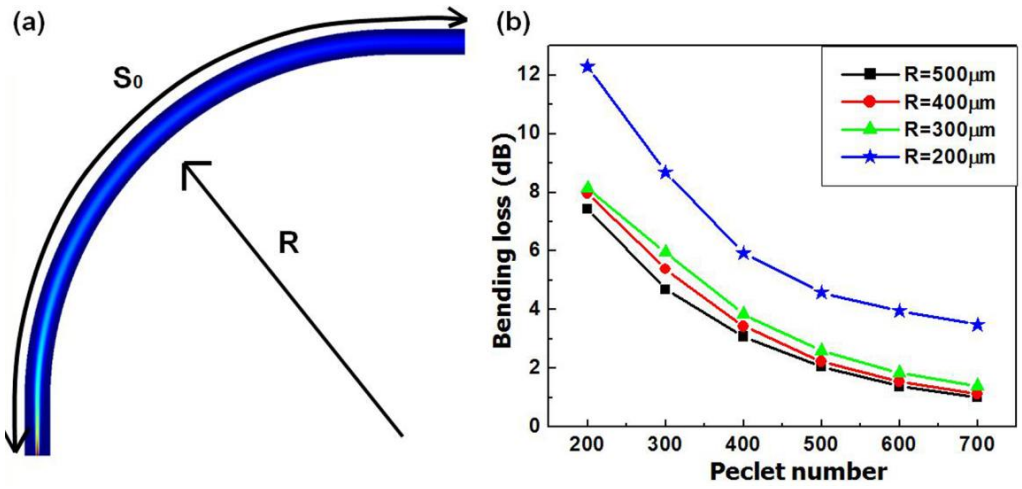

Figure 2.4 (a) Refractive index profile in the curved channel with R = 500 μm and S_0 = 500 μm at *Pe* = 600 (b) Bending loss at different Peclet numbers and different radii.

Diffusion of the liquid core in the curved liquid waveguide is faster than that in the straight liquid waveguide because of the deviation of flow velocity at the curve ("racetrack effect" [21]). Therefore two critical factors, bending radius and diffusion, make the optical power loss in the curved liquid waveguide more considerable than the straight one. At the same downstream distance, 500 μm, and Peclet number, *Pe* = 600, the straight liquid waveguide had an attenuation value of 0.19 dB while the 500 μm radius bend had 1.38 dB. Thus high Peclet number is recommended to minimize the bending loss in the liquid waveguide system with curves.

2.5 Results and discussion: liquid-to-solid light coupling

As mentioned above, optical coupling from the liquid state waveguide to the solid state waveguide represents the critical element of any future microfluidically reconfigurable photonic system. In this paper we investigate two forms of liquid to

solid optical coupling analogous to evanescent coupling and end-fire coupling in traditional solid state waveguides. In section 4.1 we study evanescent coupling in terms of coupling length and efficiency with various refractive indices of the solid waveguides and Peclet numbers of the liquid waveguides. In section 4.2 the efficiency of liquid to solid end-fire coupling is investigated. It is demonstrated that by optimizing the Peclet number of the liquid core waveguide, its mode field can be matched to that of the solid waveguide resulting in relatively efficient coupling.

2.5.1 Evanescent coupling

Similar to evanescent coupling between solid waveguides, matching the propagation constants of the two waveguides is important for the evanescent coupling from the liquid core to solid core waveguides. The propagation constant is dependent on the geometrical dimensions and refractive index of a waveguide and thus, while remaining constant along the length of a solid core waveguide, changes as a function of downstream distance for a liquid core waveguide.

Figure 2.5(a) represents the concentration profile of the liquid waveguide as it flows along-side the test solid core waveguide. The solid waveguide has the same width as the liquid waveguide at the inlet and was located 15 μm offset from the inlet of the microchannel in the X-direction and 1 μm offset in the Y-direction. An additional flow was used from the top, a red arrow in Fig. 2.5(a), to close the gap between the liquid and solid waveguide resulting from boundary layers on the solid surface. As with the simulations above in all cases we used a 500 μm long simulation

domain. Figure 2.5(b) shows the steady state electric field profile for the case of good coupling between the liquid and solid core waveguides.

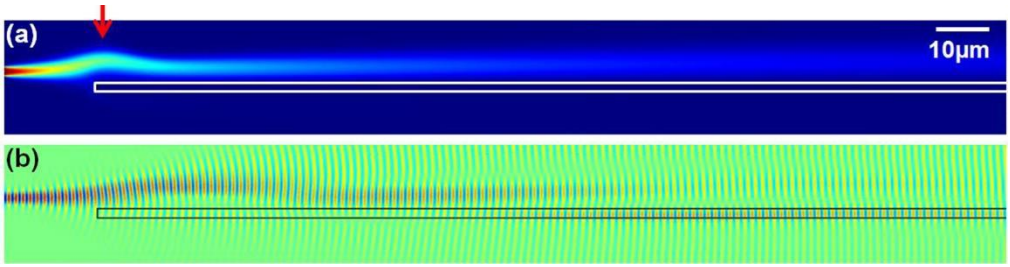

Figure 2.5 (a, b) Concentration and steady state electric field profile at *Pe* = 500. RI of liquid waveguide at the inlet was1.44 and solid waveguide was 1.37. Solid waveguide is represented as the white and black lines in Fig 2.5(a) and 2.5(b)

Before continuing to our detailed analysis, we note here an interesting property of liquid to solid phase coupling. For evanescent coupling between solid waveguides, the light coupled into the second waveguide can be coupled back into the first waveguide as an overlapped radiation mode of the first waveguide perturbs the second waveguide[22]. In contrast, the coupling from the liquid to the solid waveguide is essentially irreversible since the liquid core diffuses downstream and the propagation constants are matched only over a certain distance. We can observe the irreversible coupling in Fig. 2.5(b) in which the coupled optical energy was locked in the solid waveguide.

We performed further numerical analysis by first, investigating the evanescent coupling by varying refractive index of the solid waveguide and second, by studying the effect of Peclet number of the liquid waveguide on the evanescent coupling. Figure 2.6(a) represents the cases that the RI of the liquid waveguide was fixed at 1.44 at the inlet and Peclet number was fixed at 250 while that of the solid waveguide was varied

from 1.37 (Δn = □0.07) to 1.43 (Δn = □0.01). As mentioned above, varying the refractive index of the solid waveguide changes the required propagation constant of the liquid waveguide for light to be coupled into the solid waveguide. The light in the liquid waveguide was the fundamental mode and the coupled light in the solid waveguide was also the fundamental mode in the range investigated here.

As shown in the Fig. 2.6(a) the coupling length (*i.e.* the length measured from the start of the solid waveguide to the distance required for the light to be maximally coupled in the solid waveguide) became shorter as the RI of the solid waveguide become closer to that of the liquid waveguide. We observed that the coupling length was reduced to 10 μm when the RI solid waveguide varied from Δn = 0.07 to 0.01. Results shown in Fig 2.6(b), which shows decrease in refractive index along the liquid waveguide, confirm our findings in Fig. 2.6(a).

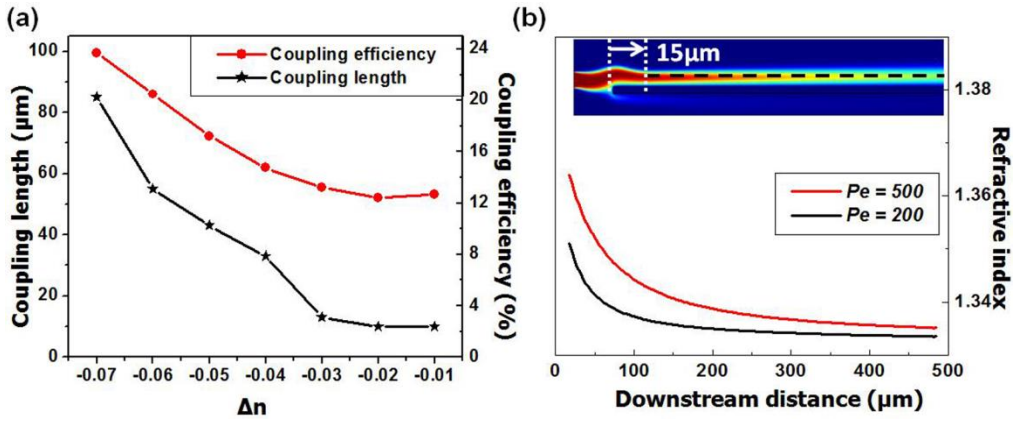

Figure 2.6 (a) Coupling length (black) and coupling efficiency (red) as a function of Δn (RI of solid waveguide – RI of liquid waveguide) at *Pe* = 250. (b) Refractive index profile along liquid waveguide at *Pe* = 200 (black) and 500 (red). The profiles were obtained along the black dotted line in the liquid waveguide and the X axis represents the downstream distance from the start of the solid waveguide.

The red line in Fig. 2.6(a) shows the coupling efficiency (defined as the ratio of the output power in the solid core waveguide to the input power of the liquid waveguide) as a function of Δn for the same Peclet number condition as those discussed above. In this fundamental mode coupling, the coupling efficiency decreased as the coupling length decreased. The shortening of the coupling length indicates that the propagation constant is matched further upstream where the refractive index changes more rapidly as seen in Fig. 2.6(b). As this matching occurs over only a short distance lower coupling efficiencies were obtained.

Figure 2.7(a) shows the coupling lengths and Fig. 2.7(b) the coupling efficiency as a function of Peclet number. The refractive index of solid waveguide (n_s) varied between $n_s = 1.37$ and $n_s = 1.40$. As shown in Fig. 2.7(a), the coupling length became longer as Peclet number becomes larger. For example, the coupling length increased from 75 μm to 100 μm when Peclet number of the liquid waveguide was changed from 200 to 500 at $n_s = 1.37$. Figure 2.7(b) shows an apparent different tendency from the previous results observed in Fig. 2.6(a) and 2.6(b) which showed reduced efficiencies as the coupling length decreased. This reversed trend is due to the faster change of propagation constants in the liquid core at higher Peclet number. The higher Peclet number resulted in the steeper gradient of the refractive index profile as seen in Fig. 2.6(b) and as a result a weakly matched propagation constant was coupled in the solid waveguide.

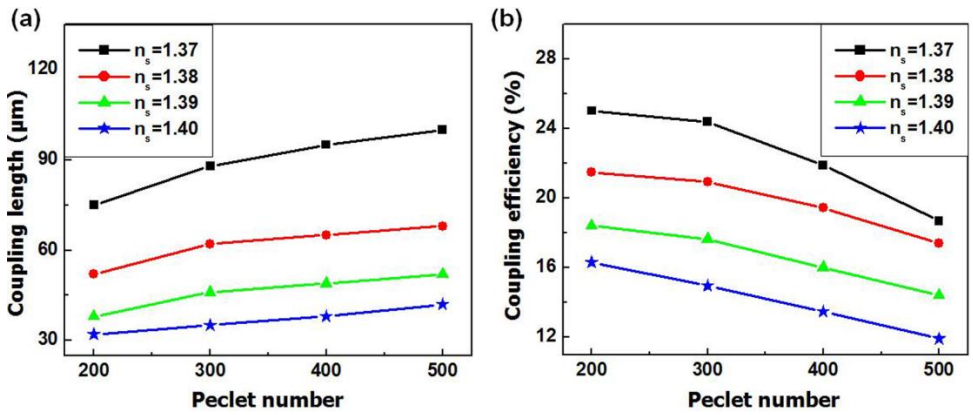

Figure 2.7 (a, b) Coupling length and coupling efficiency at different Peclet numbers (200~500) with constant refractive indices (1.37 ~1.40) of the solid waveguide

To summarize, the evanescent coupling from the liquid to the solid waveguide was effectively irreversible due to the rapid downstream change in the propagation constant in the liquid waveguide. Compared to conventional solid state couplers which have the precisely computed overlap length and fixed geometries and refractive index profiles, to obtain the pre-designed division of optical power, the performance of our two-state evanescent coupler is not restricted by its original design and thus the amount of power coupling can be tuned.

2.5.2 End-fire coupling

In section 3.1, we showed that the mode field diameter of the liquid waveguide varies according to the Peclet number of the system. Low Peclet number yielded broader concentration profiles and subsequently more weakly confined electric fields with larger mode field diameters.

Here, we exploit this tuning capability to achieve well matched MFD with that of the solid waveguide to demonstrate efficient end-fire coupling. In this case the liquid and solid waveguide were positioned along the same axis and began with the same 1.5 μm width such that the liquid waveguide enveloped the solid waveguide as shown in Fig. 2.8(a) and 2.8(c). The inlet refractive index of the liquid waveguide was 1.44 and that of the solid waveguide was the same. Figure 2.8(a) and 2.8(b) show the concentration and the steady state electric field profiles at *Pe* = 200 and Fig. 2.8(c) and 2.8(d) are at *Pe* = 800. The well matched MFD case was observed at *Pe* = 800 showing how good coupling can be obtained.

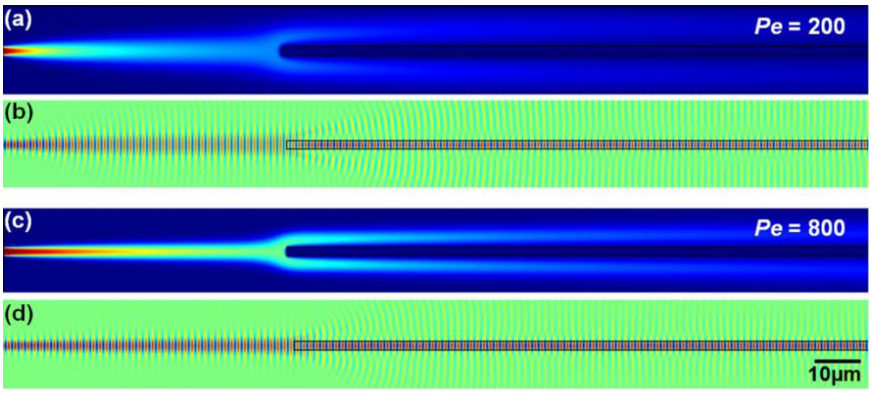

Figure 2.8. (a, b) Concentration and steady state electric field profiles at *Pe* = 200. (c, d) Concentration and steady state electric field profiles at *Pe* = 800, RI of liquid waveguide at the inlet = 1.44 and RI of solid waveguide is the same.

Figure 9(a) shows the results of the end-fire coupling efficiency into the solid waveguide as a function of liquid waveguide Peclet number. As can be seen, lower Peclet number tended to yield lower coupling efficiencies than higher ones as the mode was more disperse when it reached the edge of the waveguide for coupling. The highest coupling efficiency recorded here is 84% at *Pe* = 1000 (which was also the

highest Peclet number tested) indicating that as Peclet number of the liquid waveguide becomes higher the MFD more closely matched that of the solid waveguide. This result does not imply necessarily that higher Peclet number achieves higher coupling efficiency. Figure 9(b) shows the coupling efficiency as a function of relative refractive index Δn (RI of the solid waveguide - RI of the liquid waveguide) at different Peclet numbers. We can observer that low Peclet number has higher coupling efficiency when the RI of solid waveguide is lower than that of the liquid waveguide as can be seen in the Fig. 9(b). In Fig. 9(b) *Pe* = 200 had 57% coupling efficiency while *Pe* = 600 had 38% when the RI of the solid waveguide is 0.08 less than that of the liquid waveguide.

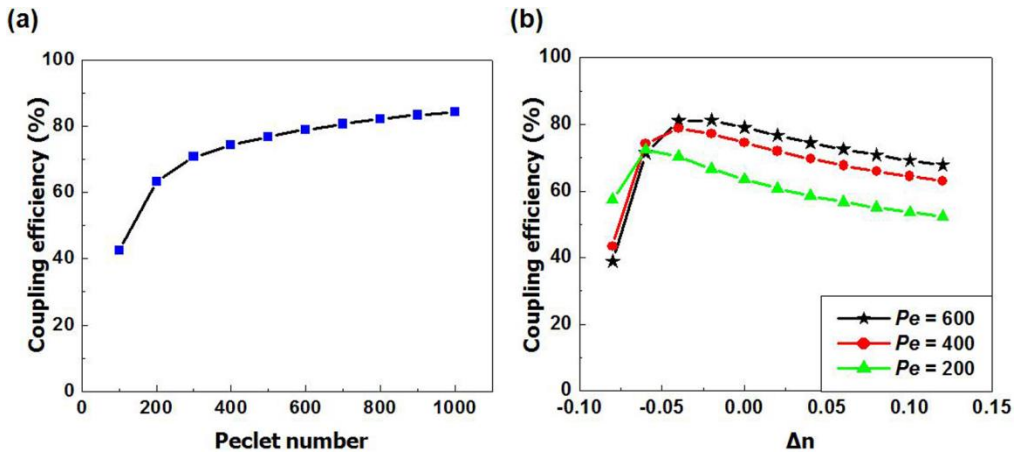

Figure 2.9 (a) Coupling efficiency at different Peclet numbers with constant RI (1.44) of solid waveguide and liquid waveguide. (b) Coupling efficiency at different RIs of solid waveguide.

This adaptability to various refractive indices of solid waveguides makes the liquid waveguide a unique mode converter. In contrast to commercial optical fibers, the liquid waveguide can adjust the MFD of optical sources to be matched to that of a

solid waveguide on a chip. Although higher coupling efficiency can be accomplished through prisms[23], gratings[24] and sophisticatedly designed converters[25], the liquid coupler has incomparable flexibility in the context of a universal converter.

2.6 Conclusions

In this paper, we have numerically investigated and characterized light propagation in liquid-core/liquid-cladding waveguides and light coupling from the liquid to the solid waveguides for cases of interest to the development of an optofluidically reconfigurable photonic system. We demonstrated that (1) instead of having a constant MFD and propagation constant as with conventional solid waveguides, the liquid waveguide's properties changed dramatically as a function of Peclet number and downstream distance due to diffusion of the liquid core, (2) that bending losses in liquid waveguide systems, even with very tight radii, could be reduced by increasing the waveguide Peclet number, (3) that evanescent coupling from the liquid to the solid waveguide was irreversible, and (4) that fluid end-fire coupling could have relatively high coupling efficiency when the tunable MFD of the liquid waveguide was matched to that of the solid waveguide. The numerical results obtained here provide valuable design data for the creation of several fluid-solid-optic components (*e.g.* optical switches, couplers, and splitters).

2.7 Acknowledgements

This work was partially supported by the Air Force Office of Scientific through an STTR grant to Illuminaria LLC. under the Reconfigurable Materials for Cellular

Electronic and Photonic Systems discovery challenge thrust and by the US National Science Foundation through grant NSF-CBET-0846489 “CAREER: Optofluidics - Fusing Microfluidics and Photonics.”

REFERENCES

1. D. Psaltis, S. R. Quake, and C. H. Yang, Developing optofluidic technology through the fusion of microfluidics and optics, Nature 442(7101), 381–386 (2006).

2. C. Monat, P. Domachuk, and B. J. Eggleton, Integrated optofluidics: A new river of light, Nat. Photonics 1(2), 106–114 (2007).

3. A. Ymeti, J. Greve, P. V. Lambeck, T. Wink, S. W. van Hövell, T. A. M. Beumer, R. R. Wijn, R. G. Heideman, V. Subramaniam, and J. S. Kanger, Fast, ultrasensitive virus detection using a Young interferometer sensor, Nano Lett. 7(2), 394–397 (2007).

4. X. L. Mao, S. C. S. Lin, M. I. Lapsley, J. J. Shi, B. K. Juluri, and T. J. Huang, Tunable Liquid Gradient Refractive Index (L-GRIN) lens with two degrees of freedom, Lab Chip 9(14), 2050–2058 (2009).

5. X. Q. Cui, L. M. Lee, X. Heng, W. W. Zhong, P. W. Sternberg, D. Psaltis, and C. H. Yang, Lensless high-resolution on-chip optofluidic microscopes for Caenorhabditis elegans and cell imaging, Proc. Natl. Acad. Sci. U.S.A. 105(31), 10670–10675 (2008).

6. S. Mandal, X. Serey, and D. Erickson, Nanomanipulation using silicon photonic crystal resonators, Nano Lett. 10(1), 99–104 (2010).

7. A. H. J. Yang, S. D. Moore, B. S. Schmidt, M. Klug, M. Lipson, and D. Erickson, Optical manipulation of nanoparticles and biomolecules in sub-wavelength slot waveguides, Nature 457(7225), 71–75 (2009).

8. D. B. Wolfe, R. S. Conroy, P. Garstecki, B. T. Mayers, M. A. Fischbach, K. E. Paul, M. Prentiss, and G. M. Whitesides, Dynamic control of liquid-core/liquid-cladding optical waveguides, Proc. Natl. Acad. Sci. U.S.A. 101(34), 12434–12438 (2004).

9. Z. Y. Li, Z. Y. Zhang, A. Scherer, and D. Psaltis, Mechanically tunable optofluidic distributed feedback dye laser, Opt. Express 14(22), 10494–10499 (2006).

10. X. C. Li, J. Wu, A. Q. Liu, Z. G. Li, Y. C. Soew, H. J. Huang, K. Xu, and J. T. Lin, A liquid waveguide based evanescent wave sensor integrated onto a microfluidic chip, Appl. Phys. Lett. 93(19), 193901–193903 (2008).

11. J. M. Lim, S. H. Kim, J. H. Choi, and S. M. Yang, Fluorescent liquid-core/air-cladding waveguides towards integrated optofluidic light sources, Lab Chip 8(9), 1580–1585 (2008).

12. M. Rosenauer, and M. J. Vellekoop, A versatile liquid-core/liquid-twin-cladding waveguide micro flow cell fabricated by rapid prototyping, Appl. Phys. Lett. 95(16), 163702–163705 (2009).

13. H. G. Park, C. J. Barrelet, Y. N. Wu, B. Z. Tian, F. Qian, and C. M. Lieber, A wavelength-selective photonic-crystal waveguide coupled to a nanowire light source, Nat. Photonics 2(10), 622–626 (2008).

14. J. S. Levy, A. Gondarenko, M. A. Foster, A. C. Turner-Foster, A. L. Gaeta, and M. Lipson, CMOS-compatible multiple-wavelength oscillator for on-chip optical interconnects, Nat. Photonics 4(1), 37–40 (2010).

15. A. J. Chung, E. Jung, and D. Erickson, A new form of reconfigurable material using optofludic waveguides, in Proceedings of Micro- Total Analysis System, (Jeju, Korea, 2009), pp. 198–200.

16. D. Lide, ed., Handbook of Chemistry of Physics, 79th ed. (CRC Press, 1999).

17. D. Marcuse, TE modes of graded-index slab waveguides, IEEE J. Quantum Electron. 9(10), 1000–1006 (1973).

18. C. R. Pollock, Fundamentals of Optoelectronics (Richard D. Irwin, INC., 1995).

19. S. Kawakami, M. Miyagi, and S. Nishida, Bending losses of dielectric slab optical waveguide with double or multiple claddings: theory, Appl. Opt. 14(11), 2588–2597 (1975).

20. K. Thyagarajan, M. R. Shenoy, and A. K. Ghatak, Accurate numerical method for the calculation of bending loss in optical waveguides using a matrix approach, Opt. Lett. 12(4), 296–298 (1987).

21. C. H. Tsai, C. H. Tai, L. M. Fu, and F. B. Wu, Experimental and numerical analysis of the geometry effects of low-dispersion turns in microfluidic systems, J. Micromech. Microeng. 15(2), 377–385 (2005).

22. A. W. Snyder, and J. D. Love, Optical waveguide Theory (Chapman and Hall, 1983).

23. K. S. Chiang, and S. Y. Cheng, Technique of applying the prism-coupler method for accurate measurement of the effective indices of channel waveguides, Opt. Eng. 47(3), 034601–034604 (2008).

24. B. Wang, J. H. Jiang, and G. P. Nordin, Compact slanted grating couplers, Opt. Express 12(15), 3313–3326 (2004).

25. V. R. Almeida, R. R. Panepucci, and M. Lipson, Nanotaper for compact mode conversion, Opt. Lett. 28(15), 1302–1304 (2003).

CHAPTER 3

CONTINUOUS OPERATION OF A HYBRID SOLID-LIQUID STATE RECONFIGURABLE PHOTONI SYSTEM WITHOUT RESUPPLY OF LIQUIDS

3.1 Abstract

Optofluidics offers a number of potentially transformative advantages for photonic systems. At present however there are a number of technological roadblocks that prevent the practical integration of liquid-state elements into traditional high-speed solid-state photonic systems. Two of the most important of these are the need for continuous resupply of liquids and the difficulty in shuttling light between the liquid- and solid-states. In this paper we present an integrated system that solves both these problems. For the first time we demonstrate direct evanescent and end-fire coupling between liquid- and solid-state waveguides and an on-chip fluid core/cladding separation and recirculation system that reduces the consumption of liquids more than 200 fold over the state of the art. The device is operated continuously for over 20hrs without performance degradation or requiring the replenishment of liquids. We believe that our system represents an important step towards the development of practical optofluidically enabled photonic systems.

*Reprinted by permission of the Royal Society of Chemistry with permission from Erica E. Jung and David Erickson, "Continuous operation of a hybrid solid-liquid state reconfigurable photonic system without resupply of liquids", *Lab-on-a-Chip*, **12**, 2575-2579 (2012), DOI: 10.1039/c2lc40191f

3.2 Introduction

The use of microfluidic components for light handling in optical systems was one of the early concepts that led to the formation of optofluidics [1-5] as a field. This idea has resulted in a number of novel technologies including: liquid-state optical lenses [6-9], dye lasers [10, 11], and liquid-core/liquid-cladding optical waveguides [12-15]. Broadly speaking, the major advantages offered by liquid-state photonic elements are that: they can be physically adapted on-the-fly over very large distances, they have widely tunable optical properties, and the inherent convective processes improve heat transfer and provide better thermal stabilization [16]. Despite these advantages, it is impractical to imagine complete replacement of traditional solid-state photonic elements with liquid-state ones due their relatively low switching speed [17] and inability to perform advanced functionalities such as signal modulation [18, 19] or active filtering [20].

One approach by which one could harness the advantages of liquid-state photonic waveguides without sacrificing the performance offered by solid-state optical devices is to combine them into so-called hybrid optofluidic systems. Examples of this type of approach include the use of microfluidically adaptable liquid-state claddings for photonic crystals [21, 22] and ring resonators [23], and the use of liquid-core waveguides as physically adaptive elements in fiber-in fiber-out optical switches [24, 25]. While these preliminary demonstrations, and other similar ones [26-32], are certainly impressive, there still two major technical limitations that prevent the widespread adoption of hybrid system technology. The first is the need to continuously replenish and remove liquids from the system. Demonstrated liquid-core

wave guiding systems consume liquids at rates on the order of hundreds of milliliters per day [12] making long term autonomous operation difficult. The second major limitation is the lack of an ability to shuttle light between the liquid-state element and traditional on-chip solid-state components, like ridge waveguides. While liquid-state to liquid-state [12] and liquid-state to fiber [24, 25] transfer has been demonstrated, the mismatch in the physical size between a liquid waveguide and single mode solid state elements makes the physics of this transfer much more difficult for chip based photonics. In a recent work, we numerically demonstrated the conditions under which it is possible to achieve this coupling [33].

In this paper we present an integrated solution to these limitations leading towards more technologically practical hybrid photonic systems. We experimentally demonstrate and characterize the conditions for direct coupling between liquid-core and photonic waveguides on a silicon substrate and a novel fluidic recirculation system that eliminates the need for the resupply or removal of liquids. Tunable end-fire and evanescent coupling between the liquid- and solid-core waveguides are demonstrated for the first time. The fluidic recirculation system is enabled by the use of immiscible liquids and on-chip separation columns. We demonstrate 20-hour continuous operation of the reconfigurable photonic device and recirculation system (performing over 24,000 independent optical switching operations in that time with minimal performance degradation via the end-fire coupling over the time) and a 200-fold reduction of the volume of used liquid compared to previous studies[34].

3.3 Results and discussion

3.3.1 Device fabrication and operation

Figure 3.1a-c shows the fabrication method used to integrate the liquid and solid waveguides onto a single substrate. Briefly, standard photolithography techniques were used to fabricate a single layer of SU-8 structure that contains: the microfluidic channels to form the liquid-core waveguide, the input and output solid-core waveguides, and the separation reservoir. The patterned SU-8 layer was covered by a single PDMS sheet to seal the microfluidic channels and provide more capacity for the separation reservoir (fig. 3.1c). Further details of the fabrication procedure are provided in the Methods section. The working principle of the recirculation system and a microscopic view of the actual device are shown in fig. 3.1d and 3.1e. The recirculation was enabled by the use of immiscible liquids, DI water (RI = 1.336) as the core solution and Fluorinert electronic oil (FC-40, RI = 1.22) as the cladding. After forming the liquid waveguide, the core and cladding liquids were collected and separated in the reservoir by taking advantage of the differences in their densities and pumped back into microfluidic channels by external micropumps. Laser light (λ=488nm) was coupled from the input solid waveguide (labeled input SWG) to the adaptable liquid waveguide and then directed to the output solid waveguides (labeled output SWG) by controlling flow rates of the fluids (note that all experiments and data presented in this paper were obtained using pure DI water as a core fluid and the core fluid was doped with Rhodamine B dye for visualization purposes only). All fluid flows were manipulated via solenoid-valves which were controlled via a customized LabVIEW program.

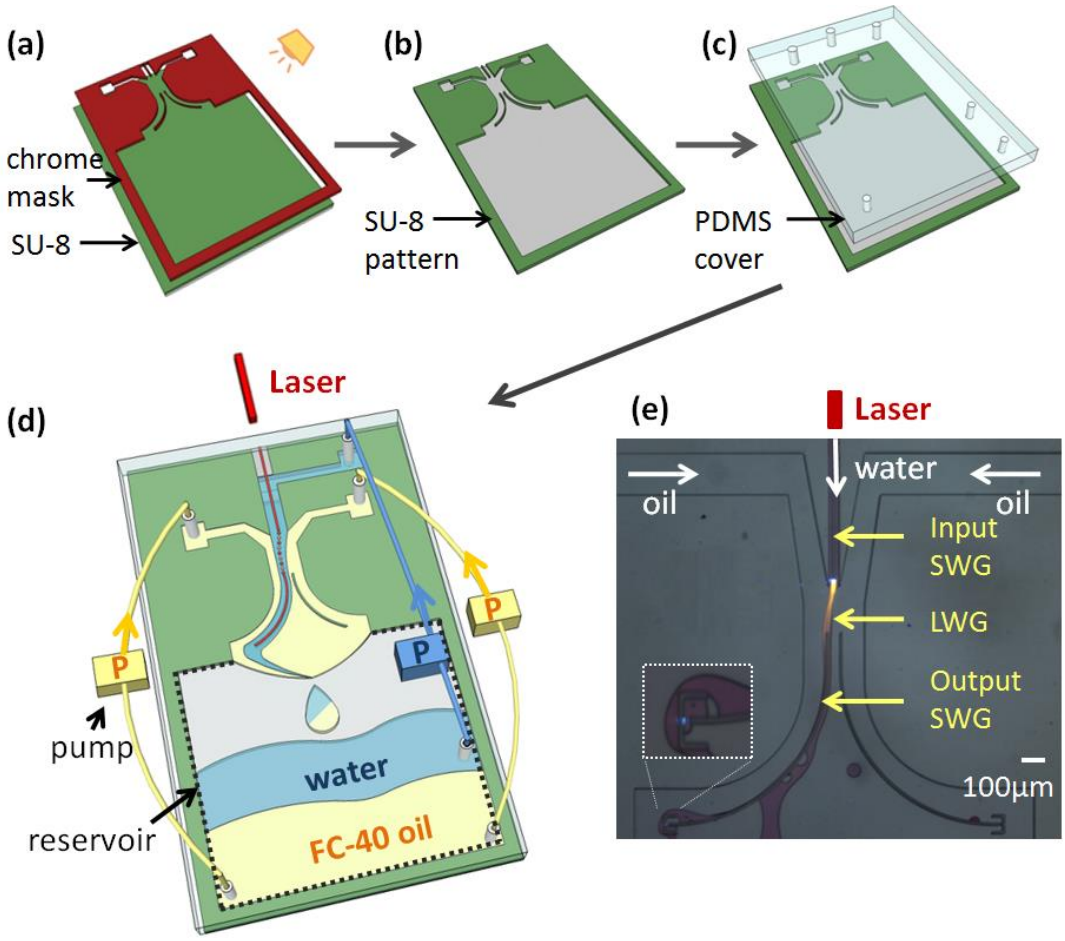

Figure 3.1 Schematic showing fabrication process used to create the hybrid chip along with a view of the physical chip during end-fire coupling. (a-c) Fabrication procedure used to form solid waveguides and microchannels on the substrate. (d) Schematic showing the operation of the fluid recirculation system. (e) Microscopic view of the actual chip performing end-fire coupling between the liquid and solid waveguides with an inset showing the coupled light (λ=488nm). (Input and output SWG: input and output solid-core waveguides, LWG: liquid-core optical waveguide).

Details about the experimental setup are provided in the Methods section. In this paper the coupling performance was evaluated and optimized by the cross-talk parameter[35] which we defined as the ratio of the output power of the coupled solid

waveguide to that of the non-coupled solid waveguide, 10 $\log[P_{coupled}/P_{non\text{-}coupled}]$. Cross-talk values were calculated integrating the pixel values over the entire surface of reflectors of the solid waveguides to minimize detection errors. Although the direct measurement of the coupling loss between the liquid and solid waveguide was not made here, analysis of the coupling efficiency between liquid and solid core waveguides is provided in our earlier work [33].

3.3.2 Liquid to solid-state end-fire coupling

Figure 3.2a shows an overview of the hybrid photonic system during operation with figure 3.2b and 3.2c illustrating the two end-fire switching states for the liquid core waveguide. Figure 3.2d shows the profile of the normalized optical intensities for the coupled (red) and non-coupled waveguides (blue) projected onto the reflectors. We observed both single mode and 2 – 3 modes on the reflector at the end of the coupled solid waveguide. Theoretically, the liquid waveguide with a width of 20μm can support as many as 50 modes. Light detected at the non-coupled waveguide was caused by scattered light from the input solid waveguide and could be reduced by the adjustment of the distance between the input and the output solid waveguides. In all experiments except the experiment for fig. 3.2(g), the coupled and non-coupled waveguides were located at 35 μm away from the center axis. Therefore we assumed that the radiation loss and the light coupled into the non-coupled waveguide are consistent in the experiments. Figure 3.2e and 3.2f illustrate the range of physical adaptability we were able to obtain with the liquid core waveguide system. To test the

effects of liquid waveguide curvature on the coupling performance, the coupled output solid waveguides were off-set between 5μm (fig. 3.2e) and 95μm (fig. 3.2f) from the center axis (equivalent to a curvature change from 10^2 to 10^3 m^{-1}) while the output solid waveguides were fixed a 35 μm from the center axis. Broadly speaking this represents a measure of the physical range over which a single element of the hybrid system can be reconfigured. Figure 3.2g shows cross-talk values as a function of the offset of the output waveguide. The cross-talk value dropped from 13dB to 6dB when the distance is increased from 5 to 65μm. As the curvature became larger (beyond 65μm offset), the radiation loss from the curved liquid waveguides became severe, consistent with what one would expect with a conventional solid waveguides [36]. Figure 3.2h-3.2i show adaptation of the width of the liquid core by changing the upstream flow conditions. This serves to change the mode profile so that it can be better matched to that of the input to the output solid core waveguide. As we decreased the applied pressure of the core flow from 70 to 17 kPa, the width of the liquid waveguide decreased from 50 to 20 μm (shown in fig. 3.2j) improving the cross-talk value from 5dB to 12dB. Due to the modal mismatch, the scattering loss at the interface of the liquid and solid waveguides is non-negligible. This loss could be reduced in future variations of the device through geometric modifications to the solid waveguides (*e.g*. adiabatically tapered solid waveguides[37]) or modulation of the refractive index of the liquid waveguide.

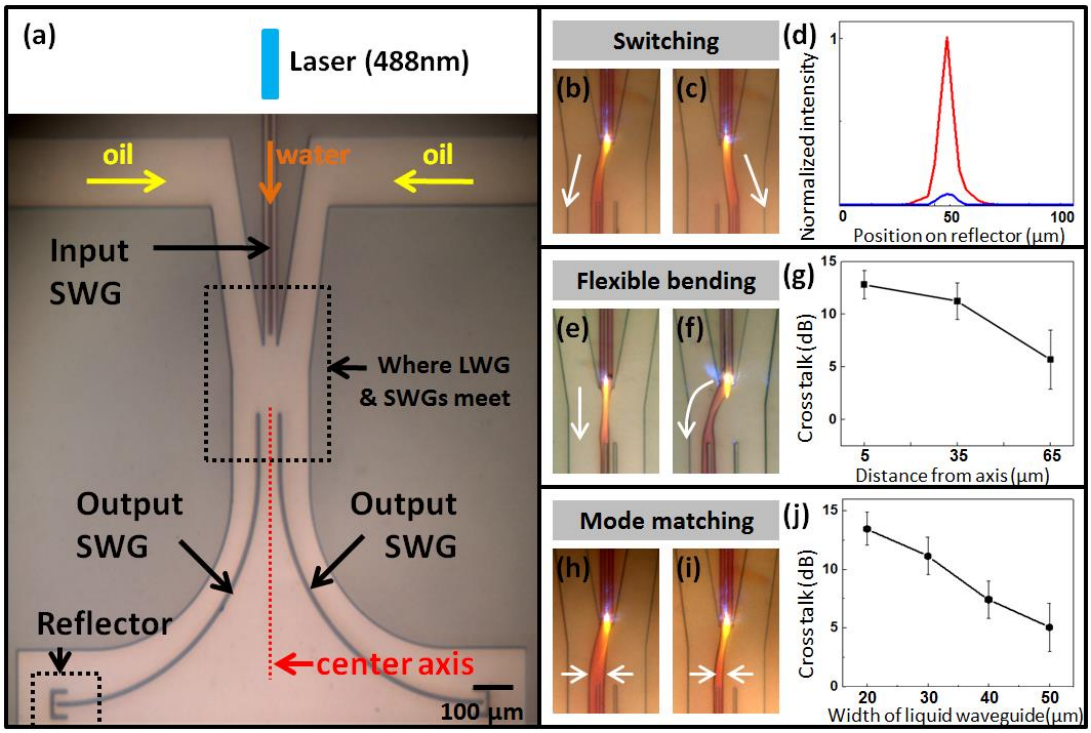

Figure 3.2 Solid to liquid to solid state end-fire coupling. (a) Microscopic view of the device without the liquid waveguide. (b-c) Switching between output waveguides. Liquid waveguide was doped with Rhodamine B dye for visualization purposes. (d) Light intensity profiles of the coupled (red) and the non-coupled (blue) solid waveguide along reflectors used to obtain cross talk. (e-f) Liquid waveguides with small and large curvatures. (g) Cross-talk values as a function of the distance from the center axis to the coupled output solid waveguide. (h-i) Effect of improved mode matching between the liquid and solid waveguides. (j) Cross-talk values as a function of the width of the liquid-core waveguide.

3.3.3 Evanescent coupling

We demonstrate here evanescent coupling between liquid- and solid-core optical waveguides for the first time. Evanescent coupling is the standard method of coupling between solid-state components and is broadly used within optical telecommunication [38, 39], biosensors [40, 41] and sustainable energy [3]. Demonstration of this type of coupling is therefore an important step in the development of practical hybrid systems.

By controlling the pressure of the cladding flow on the left side channel in fig. 3.3a, we could alter the width of the cladding flow between the liquid and the solid waveguide to change the cross-talk value. Figure 3.3d and 3.3e show the projected light on the reflector placed at the end of the output solid waveguide and cross-talk values as a function of the pressure of the cladding flow. As expected, the coupling ratio increased as the pressure of the flow decreased to narrow the gap between the liquid and the solid waveguide. At pressures lower than 7 kPa, stable physical contact between the liquid waveguide and the solid waveguide was obtained as shown in fig. 3.3b and 3.3c. We refer to this here as contact coupling. In contact coupling, the liquid waveguide becomes the cladding for the solid core after transferring light directly to the solid waveguide. When the evanescent coupling state transforms to the contact coupling state, the liquid waveguide contacts the solid waveguide resulting in no downstream flow of the left cladding stream as shown in fig. 3.3c. The transition from the evanescent to contact coupling resulted in a sudden increase of the cross-talk (6dB to 10dB). Unlike the evanescent coupling in which the coupling ratio is determined by the propagation constants of the liquid and solid waveguides, contact coupling directly transmits light across the liquid-solid interface and therefore tends to be more efficient.

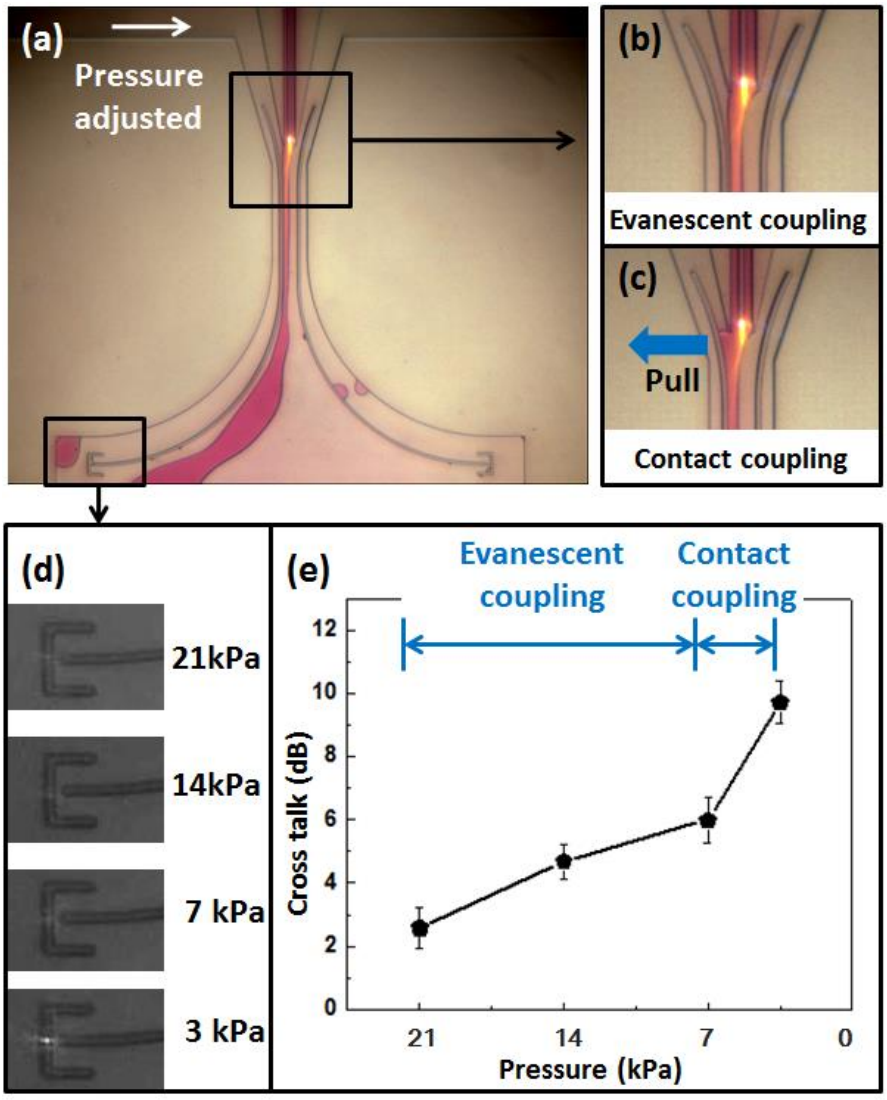

Figure 3.3 Evanescent coupling between liquid-state and solid-state waveguides. (a) Image showing a chip during coupling. (b-c) Magnified view of evanescent and contact coupling. (d) Images of the coupled light projected on the reflector as a function of the pressure of the cladding flow. (e) Cross talk values as a function of the pressure of the cladding flow showing the cross over between evanescent and contact coupling.

3.3.4 Continuous recirculation system and demonstration of long term operation

Fluidic recirculation is fundamentally important to the development of a practical hybrid system as it allows one to operate the device continuously without having to refill or remove liquids from the chip. To demonstrate the long-term operation of our device we performed the end-fire optical switching for 20 continuous hours, without requiring the resupply of liquids. As above, we measured the system performance using cross-talk values at different switching speeds (1s, 3s, and 5s). The results are shown in fig. 3.4. Supporting vides S1 and S2 show the repeated optical switching via the end fire coupling mode as observed from inside and outside the chip respectively. The fastest reconfiguration speed we could obtain was on the order of one hundred milliseconds due to the limitation in response time of the pressure-driven flow. Figure 3.4a shows images of the end fire coupling at the start and at the end of the 20 hour operational period at 1s switching speed and fig. 3.4b shows the cross talk values measured periodically during the operation. The cross-talk values increased for slower switching periods due to the more precise alignment between the liquid and solid waveguides (*i.e.* at faster switching speeds the liquid waveguide did not have time to fully settle into the optimal coupling position). No significant degradation was observed over the course of the operation for all switching speeds. While the recirculation system was capable of performing for longer durations, the experiment was stopped after 20 hours due to the thermal damage on the input solid waveguide that couples light into the chip.

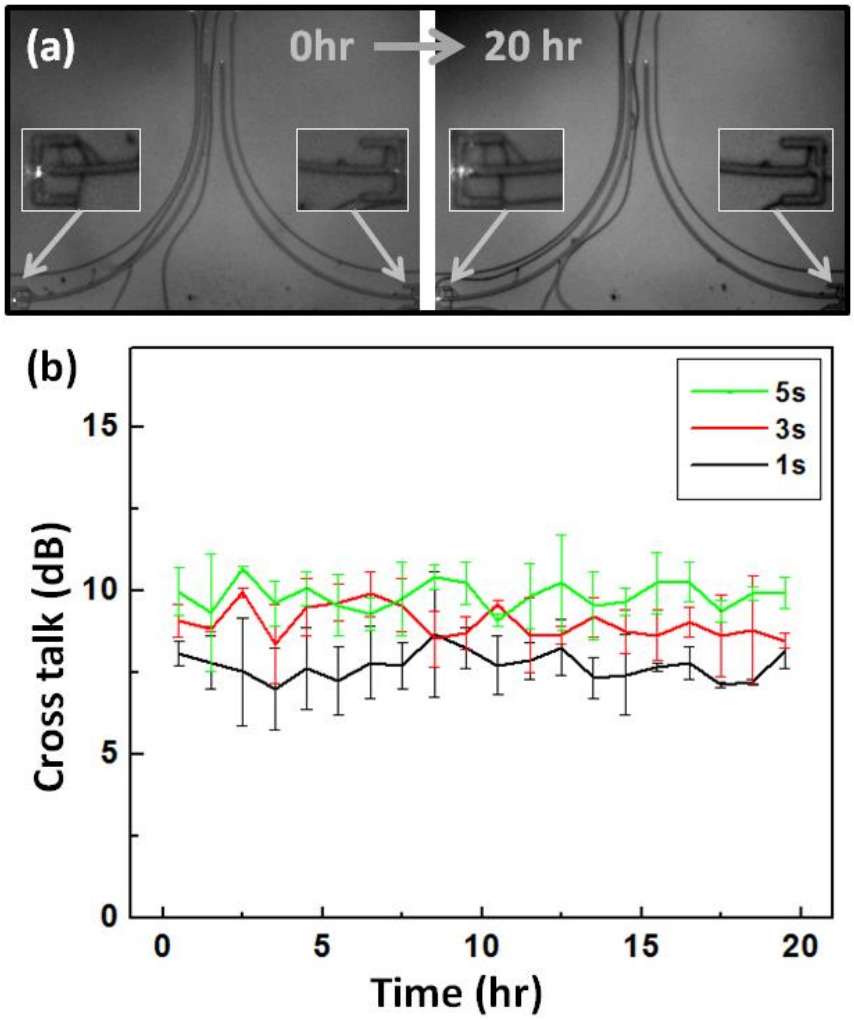

Figure 3.4 Demonstration of continuous 20-hour operation of the recirculation system. (a) Images showing end fire coupling at the start and the end of the 20-hour experiment respectively. Insets: Magnified view of reflectors where coupled lights are projected on. (b) Cross talk values with different switching speeds (1, 3, and 5s) as a function of time.

Over 20 hours, the system consumed about 200μL of working fluids due to a combination of evaporation and absorption by the permeable PDMS. The chip itself has a capacity of approximately 1mL of liquid (0.5mL of oil and 0.5mL of water) in the separation column. This loss is not fundamental to the approach but more of a consequence of the imperfect materials we used in the prototype. Better material

selection could reduce this to zero consumption. The liquid consumption compares with the 40mL/20 hours of liquid consumed by the device presented in Lim *et. al*.[34] for the same time period, representing 200-fold improvement. Even including the non-consumed portion of the fluid stored on the chip (1.2mL), this represents about 33 fold improvement over these previous works.”..

3.4 Conclusions

In this work, we have taken an important step towards the development of practical hybrid optofluidic photonic systems by demonstrating: the direct coupling between liquid-core waveguides and solid-state waveguides, and an on-chip fluidic recirculation system that vastly reduces the need for liquid replenishment enabling us to operate the devices for an extended period. We note that while the microfluidic reconfiguration demonstrated here is too slow to be used for direct signal modulation, there are a number of advantages that physical reconfiguration of the waveguiding structure enables. One of the major advantages of the physical reconfiguration of the waveguiding structure demonstrated here is that it is inherently broadband enabling the routing of light more or less independent of wavelength. Solid state methods of switching mostly rely on exploiting relatively weak refractive index modulation techniques (such as thermo-optic [42], acousto-optic [43, 44], and electro-optic effects) which must be enhanced through the use of optical resonance. Incorporating resonance necessarily narrows the range of wavelengths that can be modulated. Although physical tunability can also be obtained by micro-opto-electro-mechanical

systems (MOEMS[45, 46]), the advantage of using fluidic systems are the range of physical tunability that can be obtained (100s of micrometers) and the lack of a need to define optical elements (e.g. evanescent couplers) *a* prior. Generally speaking though, the most severe limitation of optofluidic systems to date has been the need to continuously supply and remove liquids from the devices. A non-circulating device which consumes 48mL of liquid over the course of a day[34] would require the replacement and disposal of over 0.3L of liquid each week and 17 liters over the course of a year for each element. Our demonstration of a recirculation technique that largely eliminates this need and enables of long term operation of the device without significant performance degradation is an important step towards creating practical fluid-optical systems.

3.5 Methods

3.5.1 Fabrication

The fabrication procedure is shown in fig. 3.1(a-c). Briefly, the silicon dioxide layer was grown on a silicon wafer using GSI plasma enhanced chemical vapor deposition system. SU-8 2015 (permanent epoxy negative photoresist, Microchem) was spun at 1500rpm for 40s on the silicon dioxide layer to achieve a film thickness of 30µm. Exposure of the wafer was done using a contact lithography tool and the cured photoresist was developed using a 1-Methoxy-2-propyl acetate solution (*SU-8* Developer, Microchem). The device was then diced and cleaved using a partial backside cleaving technique to create a clean coupling edge for solid waveguides on

the silicon substrate. Finally, the whole structure was covered by a sheet of PDMS (Sylgard® 184 Elastomer Kit, Dow Corning) to complete microchannels and the separation reservoir. Oxygen plasma treatment was used to bond the PDMS cover to the SU-8 structure.

3.5.2 Experimental setup

The device was mounted on the customized vertical alignment setup to separate oil (3M Fluorinert electronic liquid FC-40, density = 1855kg/m^3) and water (density = 1000kg/m^3) in the separation reservoir. Laser light (λ=488nm) was coupled from a single mode optical fiber (Thorlabs SM450) to the input solid waveguide through the free-space coupling. Images were recorded by a CCD camera (Sony XCD-X710 Firewire) mounted on the vertical microscope setup. Optical power coupled into the output solid waveguides was visualized by micro reflectors fabricated at the end of output solid waveguides.

3.6 Acknowledgements

This work was partially supported by the Air Force Office of Scientific Research through an STTR grant to Illuminaria LLC. under the Reconfigurable Materials for Cellular Electronic and Photonic Systems discovery challenge thrust, and by the US National Science Foundation through grant NSF-CBET-0846489 "CAREER: Optofluidics - Fusing Microfluidics and Photonics." The authors appreciate access and the use of the facilities of the Cornell Nanofabrication Facility (CNF).

REFERENCES

1. Psaltis, D., S.R. Quake, and C.H. Yang, *Developing optofluidic technology through the fusion of microfluidics and optics.* Nature, 2006. **442**(7101): p. 381-386.
2. Monat, C., P. Domachuk, and B.J. Eggleton, *Integrated optofluidics: A new river of light.* Nature Photonics, 2007. **1**(2): p. 106-114.
3. Erickson, D., D. Sinton, and D. Psaltis, *Optofluidics for energy applications.* Nature Photonics, 2011. **5**(10): p. 583-590.
4. Schmidt, H. and A.R. Hawkins, *The photonic integration of non-solid media using optofluidics.* Nature Photonics, 2011. **5**(10): p. 598-604.
5. Fan, X.D. and I.M. White, *Optofluidic microsystems for chemical and biological analysis.* Nature Photonics, 2011. **5**(10): p. 591-597.
6. Krupenkin, T., S. Yang, and P. Mach, *Tunable liquid microlens.* Applied Physics Letters, 2003. **82**(3): p. 316-318.
7. Pang, L., et al., *Set of two orthogonal adaptive cylindrical lenses in a monolith elastomer device.* Optics Express, 2005. **13**(22): p. 9003-9013.
8. Mao, X.L., et al., *Hydrodynamically tunable optofluidic cylindrical microlens.* Lab on a Chip, 2007. **7**(10): p. 1303-1308.
9. Tang, S.K.Y., C.A. Stan, and G.M. Whitesides, *Dynamically reconfigurable liquid-core liquid-cladding lens in a microfluidic channel.* Lab on a Chip, 2008. **8**(3): p. 395-401.

10. Li, Z.Y., et al., *Single mode optofluidic distributed feedback dye laser.* Optics Express, 2006. **14**(2): p. 696-701.

11. Song, W.Z. and D. Psaltis, *Pneumatically tunable optofluidic dye laser.* Applied Physics Letters, 2010. **96**(8).

12. Wolfe, D.B., et al., *Dynamic control of liquid-core/liquid-cladding optical waveguides.* Proceedings of the National Academy of Sciences of the United States of America, 2004. **101**(34): p. 12434-12438.

13. Seow, Y.C., S.P. Lim, and H.P. Lee, *Tunable optofluidic switch via hydrodynamic control of laminar flow rate.* Applied Physics Letters, 2009. **95**(11).

14. Lee, K.S., et al., *Three-dimensional microfluidic liquid-core/liquid-cladding waveguide.* Applied Physics Letters, 2010. **97**(2).

15. Yang, Y., et al., *A tunable 3D optofluidic waveguide dye laser via two centrifugal Dean flow streams.* Lab on a Chip, 2011. **11**(18): p. 3182-3187.

16. Levy, U. and R. Shamai, *Tunable optofluidic devices.* Microfluidics and Nanofluidics, 2008. **4**(1-2): p. 97-105.

17. Hache, A. and M. Bourgeois, *Ultrafast all-optical switching in a silicon-based photonic crystal.* Applied Physics Letters, 2000. **77**(25): p. 4089-4091.

18. Xu, Q.F., et al., *Micrometre-scale silicon electro-optic modulator.* Nature, 2005. **435**(7040): p. 325-327.

19. Levy, J.S., et al., *CMOS-compatible multiple-wavelength oscillator for on-chip optical interconnects.* Nature Photonics, 2010. **4**(1): p. 37-40.

20. Park, H.G., et al., *A wavelength-selective photonic-crystal waveguide coupled to a nanowire light source.* Nature Photonics, 2008. **2**(10): p. 622-626.

21. Erickson, D., et al., *Nanofluidic tuning of photonic crystal circuits.* Optics Letters, 2006. **31**(1): p. 59-61.

22. Smith, C.L.C., et al., *Reconfigurable microfluidic photonic crystal slab cavities.* Optics Express, 2008. **16**(20): p. 15887-15896.

23. Levy, U., et al., *On-chip microfluidic tuning of an optical microring resonator.* Applied Physics Letters, 2006. **88**(11).

24. Chung, A.J. and D. Erickson, *Optofluidic waveguides for reconfigurable photonic systems.* Optics Express, 2011. **19**(9): p. 8602-8609.

25. Lim, J.M., et al., *Pneumatic control of a liquid-core/liquid-cladding waveguide as the basis for an optofluidic switch.* Applied Physics Letters, 2011. **98**(4).

26. Campopiano, S., et al., *Microfluidic sensor based on integrated optical hollow waveguides.* Optics Letters, 2004. **29**(16): p. 1894-1896.

27. Balslev, S. and A. Kristensen, *Microfluidic single-mode laser using high-order Bragg grating and antiguiding segments.* Optics Express, 2005. **13**(1): p. 344-351.

28. Diehl, L., et al., *Microfluidic tuning of distributed feedback quantum cascade lasers.* Optics Express, 2006. **14**(24): p. 11660-11667.

29. Zhu, H.Y., et al., *Analysis of biomolecule detection with optofluidic ring resonator sensors.* Optics Express, 2007. **15**(15): p. 9139-9146.

30. Yin, D.L., et al., *Planar optofluidic chip for single particle detection, manipulation, and analysis.* Lab on a Chip, 2007. **7**(9): p. 1171-1175.

31. Lau, A.Y., L.P. Lee, and J.W. Chan, *An integrated optofluidic platform for Raman-activated cell sorting.* Lab on a Chip, 2008. **8**(7): p. 1116-1120.

32. Schonbrun, E., P.E. Steinvurzel, and K.B. Crozier, *A microfluidic fluorescence measurement system using an astigmatic diffractive microlens array.* Optics Express, 2011. **19**(2): p. 1385-1394.

33. Jung, E.E., A.J. Chung, and D. Erickson, *Analysis of liquid-to-solid coupling and other performance parameters for microfluidically reconfigurable photonic systems.* Optics Express, 2010. **18**(11): p. 10973-10984.

34. Lim, J.M., et al., *Fluorescent liquid-core/air-cladding waveguides towards integrated optofluidic light sources.* Lab on a Chip, 2008. **8**(9): p. 1580-1585.

35. Phillips, M.R. and D.M. Ott, *Crosstalk due to optical fiber nonlinearities in WDM CATV lightwave systems.* Journal of Lightwave Technology, 1999. **17**(10): p. 1782-1792.

36. Pollock, C.R., *Fundamentals of Optoelectronics.* Richard D. Irwin, INC., 1995.

37. Kasaya, K., et al., *A SIMPLE LATERALLY TAPERED WAVE-GUIDE FOR LOW-LOSS COUPLING TO SINGLE-MODE FIBERS.* Ieee Photonics Technology Letters, 1993. **5**(3): p. 345-347.

38. Chollet, F., M. de Labachelerie, and H. Fujita, *Compact evanescent optical switch and attenuator with electromechanical actuation.* Ieee Journal of Selected Topics in Quantum Electronics, 1999. **5**(1): p. 52-59.

39. Lira, H.L.R., S. Manipatruni, and M. Lipson, *Broadband hitless silicon electro-optic switch for on-chip optical networks.* Optics Express, 2009. **17**(25): p. 22271-22280.

40. Blair, S. and Y. Chen, *Resonant-enhanced evanescent-wave fluorescence biosensing with cylindrical optical cavities.* Applied Optics, 2001. **40**(4): p. 570-582.

41. Yang, A.H.J., et al., *Optical manipulation of nanoparticles and biomolecules in sub-wavelength slot waveguides.* Nature, 2009. **457**(7225): p. 71-75.

42. Camargo, E.A., H.M.H. Chong, and R.M. De la Rue, *2D Photonic crystal thermo-optic switch based on AlGaAs/GaAs epitaxial structure.* Optics Express, 2004. **12**(4): p. 588-592.

43. Verluise, F., et al., *Amplitude and phase control of ultrashort pulses by use of an acousto-optic programmable dispersive filter: pulse compression and shaping.* Optics Letters, 2000. **25**(8): p. 575-577.

44. Courjal, N., et al., *Acousto-optically tunable lithium niobate photonic crystal.* Applied Physics Letters, 2010. **96**(13).

45. Lin, L.Y., E.L. Goldstein, and R.W. Tkach, *On the expandability of free-space micromachined optical cross connects.* Journal of Lightwave Technology, 2000. **18**(4): p. 482-489.

46. Lin, L.Y. and E.L. Goldstein, *Opportunities and challenges for MEMS in lightwave communications.* Ieee Journal of Selected Topics in Quantum Electronics, 2002. **8**(1): p. 163-172.

CHAPTER 4

SLAB WAVEGUIDE PHOTOBIOREACTORS FOR MICROALGAE BASED BIOFUEL PRODUCTION

4.1 Abstract

Microalgae are one of the most promising feedstocks for sustainable biofuel production. At present however there are a number of challenges that limit the economic viability of the process. Two of the major challenges are the non-uniform distribution of light in photobioreactors and the inefficiencies associated with traditional biomass processing. To address the latter limitation, a number of studies have demonstrated organisms that directly secrete fuels without requiring organism harvesting. In this paper we demonstrate a novel optofluidic photobioreactor that can help address the light distribution challenge while being compatible with these chemical secreting organisms. Our approach is based on light delivery to surface bound photosynthetic organisms through the evanescent field of an optically excited slab waveguide. In addition to characterizing organism growth rates in the system, we also show here, for the first time, that the photon usage efficiency of evanescent field illumination is comparable to the direct illumination used in traditional photobioreactors. We also show that the stackable nature of the slab waveguide approach could yield a 12 fold improvement in the volumetric productivity.

---

*Reprinted by permission of the Royal Society of Chemistry with permission from Erica E. Jung, Michael Kalontarov, Devin F. R. Doud, Matthew D. Ooms, Largus T. Angenent, David Sinton, and David Erickson, "Slab waveguide photobioreactors for microalgae based biofuel production", *Lab-on-a-Chip*, **12**, 3740-3745 (2012), DOI: 10.1039/c2lc40490g

4.2 Introduction

Concerns surrounding global climate change and foreign energy dependency have led to substantial interest in increasing biofuel production. Biofuels can be produced from a number of different feedstocks including corn, soybean, canola and palm oil. As described by Chisti[1], meeting 50% of the US transport fuel demands with current biodiesel production technology from these feedstocks would require more than 100% of the existing US cropping area. By contrast, microalgae could meet this demand with sunlight collected from between 1% and 3% of this land[1]. This vast difference in required land space comes from the fact that microalgae have high oil yield (10 to 30 times higher than oil palm which is the next highest-yielding oil crop[1]) and the fastest growth rate among plants (their doubling time is measured in hours[2]).

Despite these advantages, there are major challenges that prevent wide-spread, commercially viable, microalgae-derived biofuel production. One of the major ones is the non-uniform distribution of light within existing photobioreactors[3] (*e.g.* open-to-air pond reactors or closed-systems tube reactors[4-6]). In dense microalgae cultures shading of incoming light by the algae themselves prevents light penetration into the deeper regions of the reactor. This results in overexposure of the organisms near the reactor surface and underexposure of the organisms below[7]. Overexposure generates reactive oxygen species capable of damaging photosynthetic machinery and underexposure provides insufficient light to sustain high volumetric productivities[8, 9]. To better distribute light within photobioreactors, innovative designs that incorporate larger surface areas[10], enhanced light-scattering by integrating light

guiding structures[11, 12], and surface plasmon based light backscattering using silver nanoparticles[13] have been proposed and demonstrated.

A second major challenge is in traditional biomass processing (*e.g.* dewatering and filtering to harvest the microalgae and cell disruption to extract the oil[14, 15]). Algal harvesting contributes to 20–30% of the total biomass production cost[16, 17] and the oil extraction from algae requires expensive chemicals and energy intensive processes[17]. To address these problems, a number of studies have generated genetically modified bacteria that directly secrete fuels, or chemical precursors to fuels, without requiring the biomass itself to be processed[18, 19]. For example, Atsumi *et al*.[20, 21] have demonstrated the production of isobutyraldehyde (a precursor to isobutanol) directly from a modified unicellular photosynthetic bacterium *Synechococcus elongatus* PCC7942. While this approach can provide a potential solution to the economic limitation of biomass processing, commercialization of this technique is limited by current photobioreactor architecture which is designed for the biomass production, not for direct fuel production.

The combination of microfluidic transport and guided wave optics that is the hallmark of Optofluidics[22] may provide a combined solution to these limitations. A recent review article by Erickson, Sinton and Psaltis[23] proposed a technique incorporating the use of waveguiding structures to deliver light via evanescent waves to photosynthetic organisms and microfluidics to introduce reactants and remove products. Figures 4.1(a) and 4.1(b) illustrate the evanescent excitation approach. Briefly, when light is guided through a waveguiding structure, an evanescent field is generated on its surface and decays exponentially a few hundred nanometers into the

surrounding media. Such a method could take advantage of coupling light directly into the photosynthetic machinery near the surface of the organism rather than illuminating the entire system. Moreover, synergetic effects can be expected by incorporating the evanescent excitation with the genetically modified bacteria that produce fuel directly. Use of these organisms reduces the need for biomass harvesting and having them fixed on a surface facilitates the controlled transport of carbon to the organisms and extraction of oxygen, fuel, and potentially restrictive endproducts. The first demonstration of evanescent field derived photosynthesis was reported by Ooms *et al.*[24] in 2012. They demonstrated that the evanescent excitation generated by the total internal reflection of light off a prism can be used to direct light into the photosynthetic membrane of *Synechococcus elongatus* ATCC 33912 and drive photosynthesis. To date however this effect has not been demonstrated using a waveguiding system that is compatible with upscaling to a pilot scale photobioreactor.

Here, for the first time, we demonstrate and characterize photosynthetic growth in the evanescent field of a slab waveguide. As part of this we also demonstrate quantitatively that the optical energy consumed by *Synechococcus elongatus* PCC7942 using evanescent illumination is as efficient as a direct illumination method. The advantages of using slab waveguides are that they are easily stackable inside a reactor and could result in dense cultures that minimize shading effects and facilitate mass transport in the interstitial space between the waveguides. As outlined in our previous review[23] increases in culture density can result in cost-effective bioreactors with lower operational costs and reduced water and energy consumption.

4.3 Results and discussion

In all of our experiments, *Synechococcus elongatus* PCC7942 (unicellular cyanobacteria, 1μm in diameter and 5μm in length) provided by Liao group at UCLA was used. This cyanobacterium, also known as blue-green algae, belongs to a phylum of bacteria that harvest optical energy for photosynthesis using photosynthetic thylakoid membranes peripherally located within a few hundred nanometers of their outer surfaces[25]. A number of recent studies have suggested the potential application of cyanobacteria for the generation of clean energy via converting sunlight into biomass[26, 27], electricity[28] and chemicals such as isobutyraldehyde[21] and ethanol[19].

Figure 4.1(c) shows the conceptual schematic of the optofluidic slab waveguide photobioreactor used here. The PDMS chamber containing the *S. elongatus* culture was fabricated from a plastic mold (width of 1cm, length of 4.5cm, and height of 6mm). A coverslip (width of 2.5cm, length of 6cm, and thickness of 150 μm) was used as the slab waveguide and support for the PDMS chamber. Although sunlight or broadband illumination could be coupled into the waveguides from lens type solar collectors[29, 30] or luminescent solar concentrators[31], for this work a laser was used as a light source to ease the optical coupling and facilitate quantification of the results. The laser light (laser diode, Newport LPM660-30C) used had a wavelength of 660nm, which is within the range of the photosynthetically active radiation (PAR: λ=400-700nm). To block the scattered, uncoupled light from entering the reactor, the clear PDMS chamber was surrounded by a carbon black embedded PDMS layer (C-PDMS layer) with a thickness of 5mm and the coverslip was placed on a slide glass

wrapped with black tape. No transmitted light could be detected behind the C-PDMS layer. The preculture was grown in standard BG11 medium under a fluorescent lamp as described previously[32, 33].

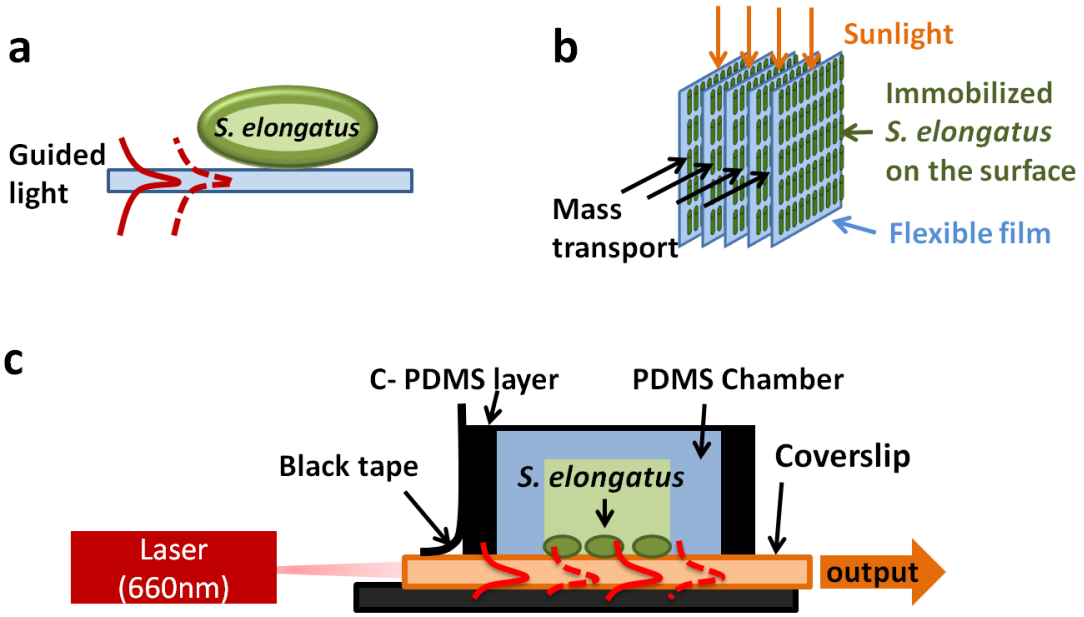

Figure 4.1 Schematic showing evanescent illumination of ***S. elongatus***, the stackable slab waveguide photobioreactor concept, and the experimental device used here (a) ***S. elongatus*** on the surface of the waveguiding structure obtain optical energy from the evanescent field of the guided light. (b) Slab waveguides with immobilized *S. elongatus* on the surface can be stacked leaving a gap for fluid based reactant/product transport. (c) In this paper we use a PDMS chamber containing *S. elongatus* solution. A coverslip is used as a slab waveguide. To block scattered and transmitted light from laser, the PDMS chamber containing *S. elongatus* solution was surrounded by C-PDMS layer and black tape.

The optical density of the culture, which is proportional to the cell concentration, was used as an evaluation parameter for *S. elongatus* growth and biomass accumulation[34]. The optical density was measured at 750nm (OD_{750}) by a spectrometer (Spectramax plus 384) and normalized to the OD_{750} of fresh BG11 media. Polystyrene spectrophotometry cuvettes (Perfector Scientific) were used for all

measurements. The preculture was maintained at the exponential growth phase (*i.e.* OD_{750} to be around 0.2) by regular dilutions of the culture. To create the initial surface phase culture on the waveguide reactors were inoculated with a dilution of the preculture into the PDMS chamber through holes on top of the chamber using a syringe. We observed about 98% of *S. elongatus* in the chamber settling down onto the cover slip surface within 24hrs, resulting in a monolayer on the surface of the slab waveguide. The reactor chips were kept in the dark during this settling process to reduce carryover growth from the preculture. Although gravity based settling was sufficient for our horizontal experiments here, we note that cell adhesives[35] could be used to form bacterial layers for vertical bioreactors. Additional details of the reactor fabrication, bacteria culturing, and experimental procedures are provided in the Materials and Methods section.

Figure 4.2(a) and 4.2(b) show photographs of the slab waveguide based photobioreactors used in this study. The reactor containing *S. elongatus* solution was illuminated only by the evanescent field of the coupled laser light as shown in Figure 4.2(a). All other lights except the laser light were blocked during experiments by the C-PDMS layer around the reactor and a black plastic film cover on top of the reactor as shown in Fig 4.2(b). To evaluate the *S. elongatus* growth rate at various locations on the slab waveguide, a transparent plastic film with 1mm x 1mm grids was integrated under the chip as shown in Figure 4.2(c). Figure 4.2(d) shows sample static images of photosynthetic growth following evanescent field illumination over the course of 5 days. Here, *S. elongatus* solutions with OD_{750} of 0.2 were diluted down 1:100 to place about 100 to 150 cells/mm^2 on the slab waveguide. 5mW of laser

power was coupled into the waveguide, measured at the exit of the waveguide as shown in Figure 4.1(c).

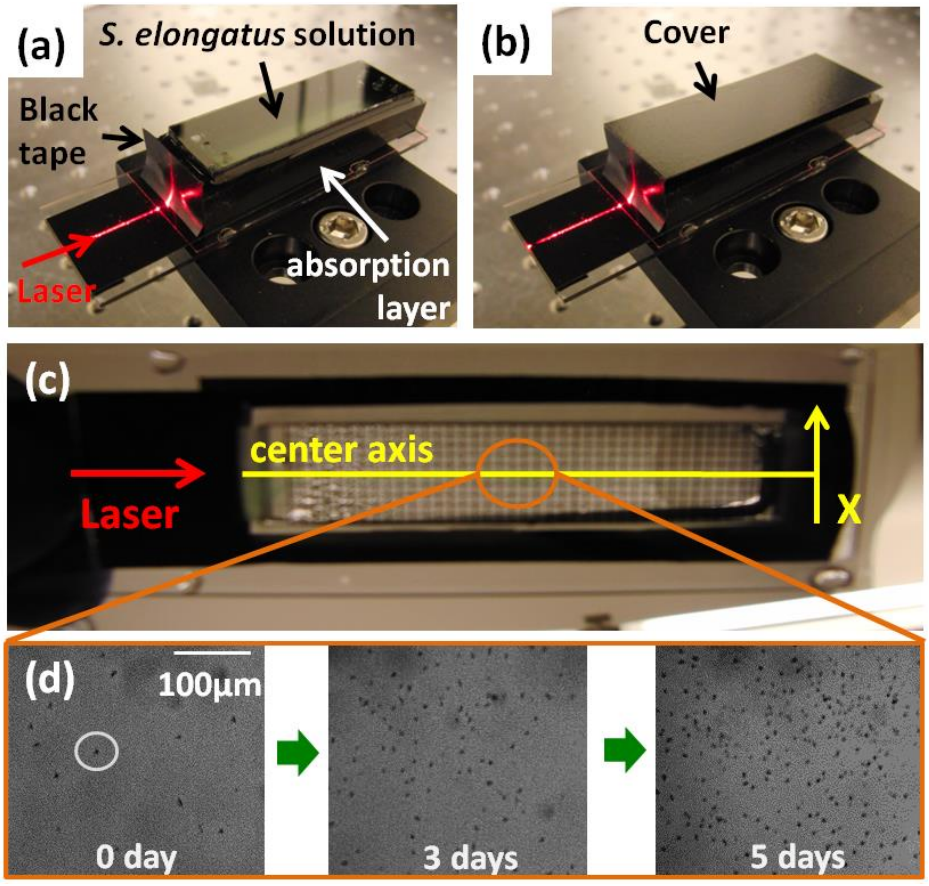

Figure 4.2 Fabricated device and ***S. elongatus*** growth through evanescent illumination. (a-b) Fabricated photobioreactor without and with a cover to block external illumination. (c) Photobioreactor with grid on the bottom for counting *S. elongatus*. (d) Experimental images showing the change in the *S. elongatus* density following 5 days of evanescent illumination.

As we will quantify below, the absorbed optical power by *S. elongatus* along the length of the waveguide was about 12μW. Under these conditions, the number of *S. elongatus* in the same region increased approximately 20 fold in 5 days. Experiments were terminated after 5 days as by that point *S. elongatus* began to grow in contact

which may influence growth. We note that although our approach is designed to work with product secreting photosynthetic organisms, here we quantify photosynthetic activity through biomass accumulation rather than fuel production due to the relative ease of making this measurement in cultures with low numbers of organisms.

The rates of *S. elongatus* growth at different locations in our reactor were characterized as shown in Figure 4.3 for 1mW and 5mW of coupled optical power. Figure 4.3(a) and 4.3(b) show the *S. elongatus* density across the width of the chip (X-direction in Figure 4.2(c)) at different locations (center axis in Figure 4.2(c), red: 1cm, yellow: 3cm, green: 5cm away from the start of the coverslip). The increase in the coupled power from 1mW to 5mW resulted in 5 fold increase in the *S. elongatus* density (Figure 4.3(a) and 4.3(b)). This indicates that the growth rate was governed by the intensity of the laser power in the range we tested. The *S. elongatus* density increased from 120 cells/mm^2 to 2900 cells/mm^2 at the center of the chip, where the evanescent field was strongest (the beam width at the entrance of the waveguide was 2mm), while the ones at the edge showed no significant change in *S. elongatus* density after 5 days. Controls with no illumination (black lines in Fig 4.3(a) and 4.3(b)) showed no growth compared to the initial density, 100 to 150 cells/mm^2. Figure 4.3(c) and 3(d) show the change in the *S. elongatus* density along the center axis of the chip as a function of time. Increase in the coupled laser power from 1mW to 5mW also increased the growth rate[36] of *S. elongatus*. The specific growth rate (*i.e.* $\ln(N_2/N_1)/(t_2-t_1)$ where N_2 and N_1 are the cell densities at time t_2 and t_1)[36] was 0.32 day^{-1} with 1mW and 0.63 day^{-1} with 5 mW (resulting in doubling times of 2.3 days and 1.1 days respectively). The *S. elongatus* located at the entrance of the chip (red)

grew faster than the ones at the exit (green). The growth rate of the *S. elongatus* at the entrance was 0.634 day^{-1} (doubling time 1.1 days) and the growth rate at the exit was 0.431 day^{-1} (doubling time 1.6 days) with the coupled laser light of 5mW. The doubling time of *S. elongatus* in standard culture is reported as several hours under optimal growth conditions[37], indicating the performance of our device can be improved by optimizing growth conditions (*e.g.* light intensity, temperature, and nutrient supply).

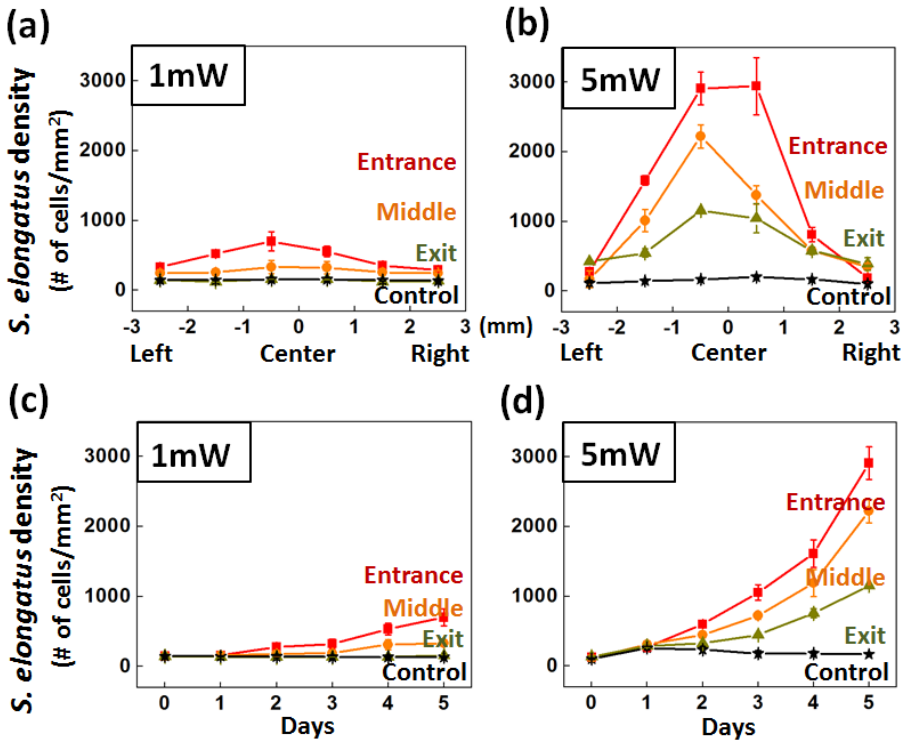

Figure 4.3 *S. elongatus* density at different locations and times in the photobioreactor. (a-b) *S. elongatus* density (number of cells/mm^2) at different locations (entrance=red, middle=orange, exit=green) across the width of the chip after 5 days of the evanescent illumination of 1mW and 5mW coupled laser power. (c) and (d) Density at different locations along the center axis of the chip as a function of time.

The difference in growth rate at the entrance and the exit of the slab waveguide was most likely the result of the lowering of the optical power density along the length of the chamber due to the expanding laser light across the width of the slab waveguide.

Figure 4.4 compares the efficiency of direct and evanescent illumination at driving the photosynthetic process. For these studies we quantify the efficiency by the ratio of the change in OD_{750} to the optical energy consumed. To measure OD_{750} in the waveguide based reactors we agitated the reactors to suspend the *S. elongatus* back into solution (from their settled state) and removed the homogenized solution for measurement. Following measurement the *S. elongatus* were returned to the chamber and allowed to settle back onto the excited waveguide. This measurement was done once per day and required removal from the illumination source for less than 10 minutes. The same devices from previous experiments were used for both evanescent and direct illumination method. For the evanescent illumination, 5mW of laser light was coupled into the slab waveguide and for the direct illumination, a yellow fluorescent lamp (discharge lamp, emission spectrum ranging from 500nm to 700nm) was used as a light source and positioned directly above the reactor. The emission spectrum of the lamp is given in the supplementary information. Figure 4.4(a) shows the change in OD_{750} values over the course of 5 days. The average OD_{750} value in the evanescently illuminated reactor changed from 0.195 to 0.225 while that in the directly illuminated reactors changed to 0.48 under 3 W/m^2 and 0.46 under 15 W/m^2 of relative optical power at 660nm. The result showed despite the 5-fold increase in the direct illumination power beyond the optimal light intensity for the *S. elongatus* growth, the OD_{750} value did not change, equivalent to no additional increase in the *S.*

elongatus concentration in the culture media. OD_{750} values of the control reactors showed no significant change over the initial value as shown in Figure 4.4(a). Figure 4.4(b) shows the total amount of optical energy absorbed by *S. elongatus* in both the direct illumination and evanescently coupled photobioreactors.

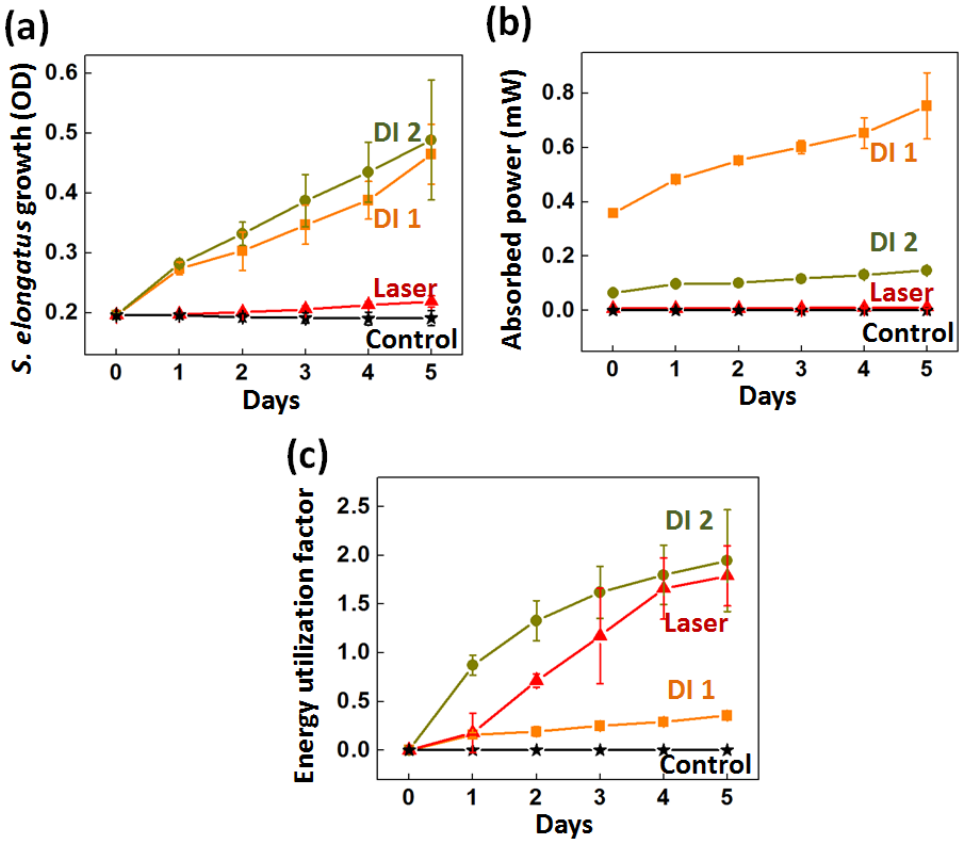

Figure 4.4 Optical energy utilization for evanescent and direct illumination methods. (a) OD_{750} values for evanescent illumination (Laser, red), direct illumination (DI1=15 W/m^2 (orange), DI2=3 W/m^2 (green) and unilluminated control (black)) as a function of time (b) Absorbed power as a function of time (c) Energy utilization factor as a function of time.

We measured 0.75mW and 0.15mW of relative optical power at 660nm were absorbed by the culture on the fifth day when the reactor was directly illuminated by 3

W/m^2 and 15 W/m^2 respectively. When the reactor was illuminated by the evanescent field 0.013mW of optical power was consumed by *S. elongatus* on the fifth day. Details of the measurement of absorbed powers are provided in the Material and Method section. The energy efficiencies of photobioreactors were evaluated by an "energy utilization factor" which we defined as the ratio of the OD_{750} change to the absorbed optical power. Figure 4.4(c) shows calculated energy utilization factors. The energy utilization factor of the evanescent illumination was similar to that of 3 W/m^2 direct illumination, while the 15 W/m^2 direct illumination was 5-fold lower than the previous two. This result implies that the optical energy utilized by *S. elongatus* to grow photosynthetically, and therefore the energy efficiency, is comparable for evanescent and direct illumination. It is possible however that the energy utilization factor of the evanescent illumination was underestimated because several hours were needed for *S elongatus* to settle on the slab waveguide to access the evanescent field after the daily OD measurement, whereas the direct illumination culture did not require this setting time. Also, given the non-uniformity of the light field, removing productive organisms for OD measurement and redistributing uniformly on the waveguide may set back growth leading to further underestimation.

The stackable nature of the slab waveguide evanescent illumination approach developed here could enable much higher volumetric productivity than existing photobioreactor designs. The volumetric productivity can be estimated by comparing the ratio of the change in OD over time (discussed above) to the volume utilized to grow the organisms. A monolayer of cells would require approximately 5 μm to grow and that the efficacy of the evanescent field to support growth is practically limited to

this region, as demonstrated by Ooms *et al*.[24]. Including the thickness of the slab waveguide used here (150 μm) and leaving space between slab waveguides for mass transport (50μm) as shown in Figure 4.1(b), total volume required to grow *S. elongatus* using the slab waveguide photobioreactor is approximately 200μm x surface area of the slab waveguide. For the proof-of-concept system demonstrated here the volumetric productivity (ΔOD_{750} / utilized volume) would be 0.03 / (200μm x surface area of the slab waveguide). For a system in which the organisms are grown on both sides of the waveguide, this value would double. The volumetric productivity of the direct illumination method would be 0.285 / (6mm x surface area). When compared the evanescent illumination with organisms on both sides of waveguide yields a 6-fold increased volumetric productivity. This could be greatly improved however by uniformly distributing light across the width of the slab waveguide. As shown in Figure 4.2 and quantified in Figure 4.3(a) and (b) in the prototype system the light is much more intense in the middle than the edges so the waveguide area is not fully utilized. Modulating the light so as to achieve the optimal growth rate over the entire slab waveguide would improve the volume productivity another 2-fold to around 12-fold improvement (for a double sided waveguide) of the direct illumination method.

4.4 Conclusions

In this work, we have demonstrated a photobioreactor that utilizes the evanescent field of a slab waveguide to culture photosynthetic organisms. We demonstrated for the first time that the optical energy consumed to grow organisms using the evanescent illumination was at least as efficient as that using the direct illumination. The

evanescent illumination method would yield a 6-12 fold improvement in the volumetric productivity. The optofluidic approach demonstrated here can provide an appropriate architecture for a new type of biofuel production reactor that utilizes the genetically modified photosynthetic organisms to produce fuel directly.

4.5 Materials and methods

4.5.1 Photosynthetic organism cultures and optical density measurements

Synecochoccus elongatus PCC7942 was used for all experiments. It was maintained in BG-11 media under fluorescent light maintained at an intensity of 30 μE $m^{-2}s^{-1}$ and maintained at room temperature. Fresh pre-culture was maintained at the exponential growth phase (*i.e.* OD_{750} to be around 0.2) by regular inoculation of the solution. Prior to any experiments the culture was kept in the dark for at least a day to reduce carryover growth from the preculture. OD_{750} values were measured using a spectrophotometer (Spectramax plus 384).

4.5.2 Reactor fabrication

The PDMS chambers were fabricated from a plastic master that was formed by laser cutting. Uncured PDMS was poured over the plastic master and cured for 2 h in an 80°C convection oven. The resulting chambers had a 2.5mL capacity (W: 1cm x L: 4.5cm x H: 6mm). The light absorption layers (C-PDMS layer) consisted of carbon black, PDMS base, and PDMS curing agent in the ratio 0.01:1:0.1 by weight[38]. The C-PDMS was poured around the cured PDMS chamber, leaving a window on top of the chamber. The C-PDMS surrounded chamber was cut out from the master to have

the 5mm thick C-PDMS layer as shown in Figure 4.2(a) and 4.2(b). The chamber was bonded to a coverslip by epoxy. PDMS chambers and coverslips used in experiments were pre-cleaned with 70% Isopropyl Alcohol (IPA).

4.5.3 Measurement of absorbed power

To quantify the amount of optical energy absorbed by *S. elongatus* growing on the surface of the waveguide, the power difference measured on the top and the bottom of the reactor filled with plain media was subtracted from that of the reactor filled with the organisms. The power absorbed by the organisms on the waveguide was measured in a similar manner. The output measured at the end of the slab waveguide when the organisms had settled on the waveguide was subtracted from the output measured when the chamber was filled with plain media.

4.6 Acknoledgements

This work was supported by the academic venture fund of the David R. Atkinson Center for Sustainable Future and a CAREER grant from the National Science Foundation (NSF) for Optofluidics – Fusing Microfluidics and Photonics (#0846489). The authors would also like to thank Liao group at UCLA for providing the *S. elongatus* strain used in this study.

REFERENCES

1. Chisti, Y., *Biodiesel from microalgae.* Biotechnology Advances, 2007. **25**(3): p. 294-306.
2. Kratz, W.A. and J. Myers, *NUTRITION AND GROWTH OF SEVERAL BLUE-GREEN ALGAE.* American Journal of Botany, 1955. **42**(3): p. 282-287.
3. Grima, E.M., et al., *Photobioreactors: light regime, mass transfer, and scaleup.* Journal of Biotechnology, 1999. **70**(1-3): p. 231-247.
4. Janssen, M., et al., *Enclosed outdoor photobioreactors: Light regime, photosynthetic efficiency, scale-up, and future prospects.* Biotechnology and Bioengineering, 2003. **81**(2): p. 193-210.
5. Posten, C., *Design principles of photo-bioreactors for cultivation of microalgae.* Engineering in Life Sciences, 2009. **9**(3): p. 165-177.
6. Lehr, F. and C. Posten, *Closed photo-bioreactors as tools for biofuel production.* Current Opinion in Biotechnology, 2009. **20**(3): p. 280-285.
7. Lee, C.-G., *Calculation of light penetration depth in photobioreactors.* Biotechnology and Bioprocess Engineering, 1999. **4**(1): p. 78-81.
8. Bosma, R., et al., *Prediction of volumetric productivity of an outdoor photobioreactor.* Biotechnology and Bioengineering, 2007. **97**(5): p. 1108-1120.
9. Grima, E.M., et al., *A study on simultaneous photolimitation and photoinhibition in dense microalgal cultures taking into account incident and averaged irradiances.* Journal of Biotechnology, 1996. **45**(1): p. 59-69.

10. Ugwu, C.U., H. Aoyagi, and H. Uchiyama, *Photobioreactors for mass cultivation of algae.* Bioresource Technology, 2008. **99**(10): p. 4021-4028.

11. Mori, K., *PHOTOAUTOTROPHIC BIOREACTOR USING VISIBLE SOLAR RAYS CONDENSED BY FRESNEL LENSES AND TRANSMITTED THROUGH OPTICAL FIBERS*, in *Scott, C. D.*1986. p. 331-346.

12. Chen, C.Y., et al., *Phototrophic hydrogen production in photobioreactors coupled with solar-energy-excited optical fibers.* International Journal of Hydrogen Energy, 2008. **33**(23): p. 6886-6895.

13. Torkamani, S., et al., *Plasmon-enhanced microalgal growth in miniphotobioreactors.* Applied Physics Letters, 2010. **97**(4).

14. Wijffels, R.H. and M.J. Barbosa, *An Outlook on Microalgal Biofuels.* Science, 2010. **329**(5993): p. 796-799.

15. Brennan, L. and P. Owende, *Biofuels from microalgae-A review of technologies for production, processing, and extractions of biofuels and co-products.* Renewable & Sustainable Energy Reviews, 2010. **14**(2): p. 557-577.

16. Grima, E.M., et al., *Recovery of microalgal biomass and metabolites: process options and economics.* Biotechnology Advances, 2003. **20**(7-8): p. 491-515.

17. Mata, T.M., A.A. Martins, and N.S. Caetano, *Microalgae for biodiesel production and other applications: A review.* Renewable & Sustainable Energy Reviews, 2010. **14**(1): p. 217-232.

18. Wahlund, T.M., T. Conway, and F.R. Tabita, *Bioconversion of CO2 to ethanol and other compounds.* Abstracts of Papers of the American Chemical Society, 1996. **212**: p. 120-FUEL.

19. Deng, M.D. and J.R. Coleman, *Ethanol synthesis by genetic engineering in cyanobacteria.* Applied and Environmental Microbiology, 1999. **65**(2): p. 523-528.

20. Atsumi, S., T. Hanai, and J.C. Liao, *Non-fermentative pathways for synthesis of branched-chain higher alcohols as biofuels.* Nature, 2008. **451**(7174): p. 86-U13.

21. Atsumi, S., W. Higashide, and J.C. Liao, *Direct photosynthetic recycling of carbon dioxide to isobutyraldehyde.* Nature Biotechnology, 2009. **27**(12): p. 1177-U142.

22. Psaltis, D., S.R. Quake, and C.H. Yang, *Developing optofluidic technology through the fusion of microfluidics and optics.* Nature, 2006. **442**(7101): p. 381-386.

23. Erickson, D., D. Sinton, and D. Psaltis, *Optofluidics for energy applications.* Nature Photonics, 2011. **5**(10): p. 583-590.

24. Ooms, M.D., et al., *Evanescent photosynthesis: exciting cyanobacteria in a surface-confined light field.* Physical chemistry chemical physics : PCCP, 2012. **14**(14): p. 4817-23.

25. Nevo, R., et al., *Thylakoid membrane perforations and connectivity enable intracellular traffic in cyanobacteria.* Embo Journal, 2007. **26**(5): p. 1467-1473.

26. Chisti, Y., *Biodiesel from microalgae beats bioethanol.* Trends in Biotechnology, 2008. **26**(3): p. 126-131.

27. Sheng, J., R. Vannela, and B.E. Rittrnann, *Evaluation of methods to extract and quantify lipids from Synechocystis PCC 6803.* Bioresource Technology, 2011. **102**(2): p. 1697-1703.

28. Pisciotta, J.M., Y. Zou, and I.V. Baskakov, *Light-Dependent Electrogenic Activity of Cyanobacteria.* Plos One, 2010. **5**(5).

29. Ono, E. and J.L. Cuello, *Design parameters of solar concentrating systems for CO2-mitigating algal photobioreactors.* Energy, 2004. **29**(9-10): p. 1651-1657.

30. Rabl, A., *COMPARISON OF SOLAR CONCENTRATORS.* Solar Energy, 1976. **18**(2): p. 93-111.

31. Giebink, N.C., G.P. Wiederrecht, and M.R. Wasielewski, *Resonance-shifting to circumvent reabsorption loss in luminescent solar concentrators.* Nature Photonics, 2011. **5**(11): p. 695-702.

32. Asato, Y., *Toward an understanding of cell growth and the cell division cycle of unicellular photoautotrophic cyanobacteria.* Cellular and Molecular Life Sciences, 2003. **60**(4): p. 663-687.

33. Ritchie, R.J., D.A. Trautman, and A.W.D. Larkum, *Phosphate uptake in the cyanobacterium Synechococcus R-2 PCC 7942.* Plant and Cell Physiology, 1997. **38**(11): p. 1232-1241.

34. Gillies, R.J., N. Didier, and M. Denton, *DETERMINATION OF CELL NUMBER IN MONOLAYER-CULTURES.* Analytical Biochemistry, 1986. **159**(1): p. 109-113.

35. Elbert, D.L., C.B. Herbert, and J.A. Hubbell, *Thin polymer layers formed by polyelectrolyte multilayer techniques on biological surfaces.* Langmuir, 1999. **15**(16): p. 5355-5362.

36. Monod, J., *THE GROWTH OF BACTERIAL CULTURES.* Annual Review of Microbiology, 1949. **3**: p. 371-394.

37. Mori, T., B. Binder, and C.H. Johnson, *Circadian gating of cell division in cyanobacteria growing with average doubling times of less than 24 hours.* Proceedings of the National Academy of Sciences of the United States of America, 1996. **93**(19): p. 10183-10188.

38. Krishnan, M. and D. Erickson, *Optically induced microfluidic reconfiguration.* Lab on a Chip, 2012. **12**(3): p. 613-621.

CHAPTER 5

STACKABLE ULTRACOMPACT PHOTOBIOREACTOR FOR MICROALGAE BASED BIOFUEL PRODUCTION

5.1 Abstract

Bench scale sstackable photobioreactors that highly improves the volumetric productivity of photobioreactors for the algae biofuel production have been demonstrated. The stackable layout demonstrated in chapter 4 has been examined in a 10 stack waveguide photobioreactor. We have applied optofluidic approaches, the evanescent illumination and light scatterings on the surface of planar waveguides, to achieve even distribution of light in the photobioreactors. The waveguide layout minimized the shading effect and therefore enabled the even growth of photosynthetic bacteria across 10 layers. Importantly, we have demonstrated the continuous fuel production by genetically modified bacteria using the bench scale photobioreactor.

5.2 Introduction

Biofuel, from ethanol, methanol to diesel, can be produced from various feedstocks. Among the promising feedstocks for sustainable biofuel production, microalgae have a number of advantages including [1]: (1) no competition for land with agricultural crops (2) high oil contents and (3) fast growth rate compared to other sources like corn,

soy, sugar cane, camellia, and rapeseed. Despite these advantages, two major challenges prevent the widespread adoption of the algae biofuel production[2]. The first is the poor distribution of sun light over photobioreactors. As the concentration of microalgae increases in culture media, it is difficult for light to penetrate into the culture media, resulting in uneven distribution of light. This shading effect is one of fundamental limitations of algae culture in current photobioreactors [3] (e.g. pond and tubular types). A number of approaches have been developed to improve the distribution of light. For instance, surface plasmon resonance generated by silver nanoparticles was employed to promote the backscattering of the incoming light[4]. The second is the costs for the maintenance (e.g. to keep the constant temperature and to avoid contaminations) and post processes (e.g. the dehydration of growth media and extraction of oil). The large volume required due to the uneven distribution of light results in high costs for the maintenance and post processes. To avoid the post processes, researchers have been developing genetically modified photosynthetic bacteria that can directly produce fuels [5, 6]. While these preliminary studies to address the two major challenges are certainly impressive, large scale algae production is not economically viable yet. In this chapter we demonstrate a novel optofluidic photobioraector that offers potential solutions for these problems.

In the previous chapter, we have demonstrated a photobioreactor that utilizes the evanescent field of a slab waveguide to improve the volumetric productivity. We demonstrated the photosynthetic bacterial growth using the evanescent illumination of the slab waveguide. We also demonstrated that the optical energy consumed to grow organisms using the evanescent illumination was at least as efficient as that using the

direct illumination. Here, we demonstrate a bench scale prototype of 10 stack photobioreactor that utilizes 10 slab waveguides for the effective microalgae based biofuel production. The optofluidic reactor is based on the delivery of light via the evanescent field and scattering lights along low-cost solid state slab waveguides. Due to the stackable nature of structure, this new approach could enable ultracompact reactors with: volume to surface area ~100x enhanced over state-of-the-art pond/enclosed reactors, more efficient solar energy-to-photosynthetic product conversion, and dramatically lower operational energy costs and water usage (due to the small size of the reactor and elimination of the need to continuously circulate the culture).

5.3 Results and discussion

We designed and fabricated a 10 stack photobioreactor as shown in Fig. 5.1(a). The reactor consists of a 3D holder to assemble ten coverslips, ten coverslips to guide coupled lights, and absorption layer made of carbon black embedded PDMS to block non-coupled lights from LED light sources. The dimensions of the reactor are 2.5cm in width, 3cm in height and 6cm in length. Each of ten layers was isolated by 3D printed barriers inside the reactor. Figure 5.1(b) shows a set up to activate the photobioreactor. Lights are coupled into both side of the reactor at an intensity of 200W/m^2. Fresh media is supplied via individually connected tubes on each layer, and waste and potentially produced fuel can be dispensed via tubes on the other side of the photobioreactor. We demonstrated that the layout of the photobioreactor and flow

system were suitable to grow bacteria in the presence of sufficient lights to drive photosynthesis. To test the photobioreactor, cyanobacteria (*Synechocysitis 6083*) were grown in the photobioreactor when the light was directly illuminated to the photobioreactor for a week (Fig. 5.1(c)).

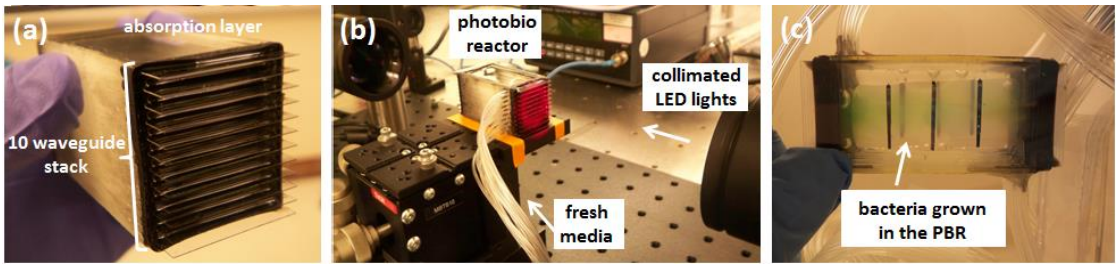

Figure 5.1. 10 stack photobioreactor (a) fabricated 10 stack photobioreactor, (b) experimental setup, (c) bacteria grown in the photobioreactor.

We initially attempted to grow bacteria through an evanescent field only that was generated on the surface of the planar waveguide. However to utilize the coupled light more efficiently and to distribute the light more evenly on the surface of the reactor, light scattering from the surface of the waveguide was employed. To achieve a maximum light scattering for the bacteria growth, several methods that modify the surface of the planar waveguide have been examined. Figure 5.2(a) represents a plain cover slip where the LED light was coupled into. Less than a detectable intensity of light was emitted from the surface of the plain cover slip. We then modified the coverslip surfaces (Fig. 5.2(b) – (d)). A cover slip was mechanically modified by forming scratches on the surface using sand papers (Fig. 5.2(b)). Also, SU-8 micro posts (1μm in diameter and 2μm in height) were fabricated on the surface by soft lithography techniques (Fig. 5.2(c)). In addition, a cover slip was etched using a glass

etching cream (Fig. 5.2(d)). Although scatterings from the modified coverslips enhanced the light intensity significantly compared to the plain cover slip as shown in the table, it was far below than the optimal light intensity for the bacterial growth (10 W/m^2-50W/m^2 at $\lambda = 635nm$). To increase the light intensity, we adapted a glass slide that has 7 times larger area than the cover slip to couple incident lights (Fig. 5.2(e)). In addition to the larger area for a better coupling of incident lights, we also integrated air claddings on both sides of the etched glass slide to maximize the scattering by larger difference in refractive indices (1.45 to 1.33 when the glass slide is cladded by water vs. 1.45 to 1 when it is cladded by air). Figure 5.2(f) shows the glass slide with air claddings illuminated by LEDs. Air claddings were fabricated by attaching the coverslips on both side of the etched glass slide using uncured PDMS. Overall, the scattering efficiency increased 50 times compared to the etched cover slips.

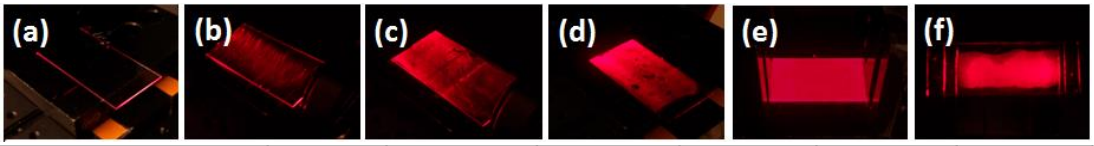

	(a) Plain	(b) Scratched	(c) SU-8 pillars	(d) Etched coverslip	(e) Etched glass slide	(f) Air cladded
Scattered light measured on top of surfaces	0	16 mW/m^2	40 mW/m^2	35 mW/m^2	200 mW/m^2	1.8 W/m^2

Figure 5.2. Modified surfaces to enhance light scattering (a) plain coverslip, (b) scratched coverslip, (c) coverslip with SU-8 pillars, (d) Etched coverslip, (e) Etched glass slide, (f) Air-cladded etched glass slide.

To optimize the bacterial growth, we have installed LEDs that are 10 times brighter than the collimated LED lights. The intensity measured on the air-cladded glass slide with the high power LEDs was 17 W/m^2. When four sheets of the glass slides were

assembled in the photobioreactor, the integrated light intensity reached up to 40 W/m^2, supplying an optimal intensity of light to cultivate bacteria.

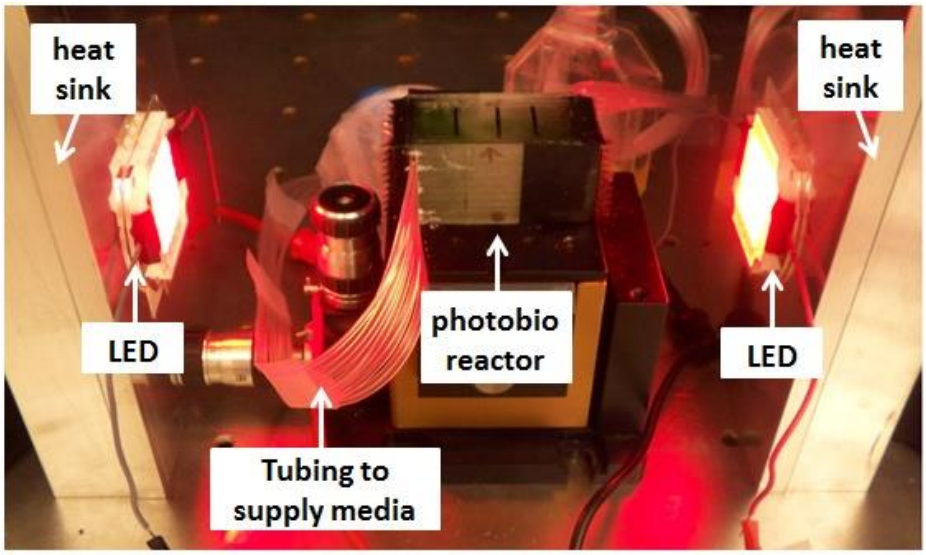

Figure 5.3 Final 10 layer reactor design currently being tested.

Figure 5.3 shows the setup of high powered LEDs and cooling systems. Bacteria solution of OD 0.006 was loaded into the photobioreactor illuminated by the coupled LED lights via the waveguides. Bacterial growth in the reactor has been monitored for 3 days. Figure 5.4 shows fluorescent images of bacteria on the surface of the first layer of the photobioreactor. Figure 5.4(a) and (b) images show the surface distribution of bacteria at 9 locations on the waveguide surface before and after 3days of the light illumination. Initially, the surface coverage was less than 1 %, however, the coverage increased to higher than 70% within 3 days. Optical density of the culture media increased from 0.006 to 0.5.

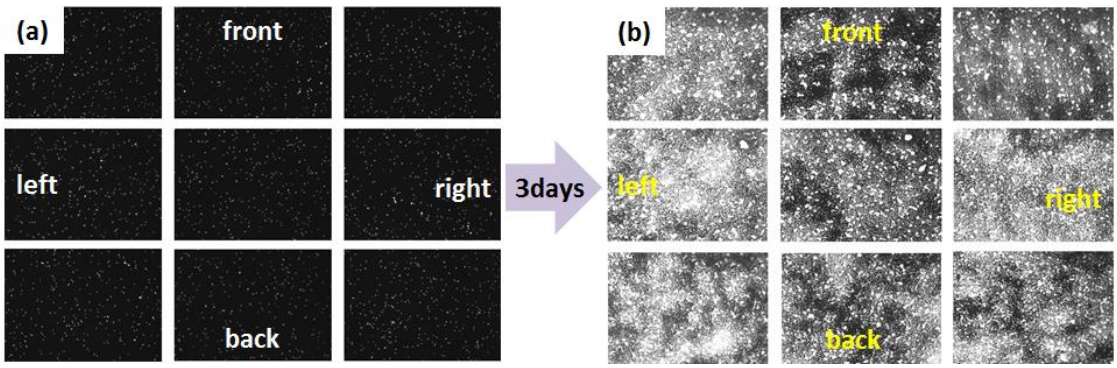

Figure 5.4 Fluorescent images of bacteria distribution on the surface of the first layer of the 10 stack photobioreactor. (a) Initial distributions of bacteria before the light illumination via slab waveguides (b) final distributions of bacteria after the light illumination via slab waveguides for 3 days

Figure 5.5(a) shows the bacteria culture grown in the photobioreactor illuminated by the LEDs for 5 days. Figure 5.5(b) shows the bacterial solution extracted from each layers which was cultured in the photobioreactor for 5 days and the control media that was cultured in the reactor kept in dark for 5 days. The bacterial solution extracted from each stack of the reactor had little variation in the optical density showing that there was no shading effect between layers. More importantly, we observed that bacteria in the photobioreactor have produced gases over the period. The gas bubbles generated in the photobioreactor were collected and analyzed daily basis and the table in fig. 5.5 shows the ethylene measured during the period using a gas chromatography. The specific production rate of the measured ethylene was between 8 µL/L/h/OD to 120 µL/L/h/OD which was 80% of the literature value [7] (155 µL/L/h/OD).

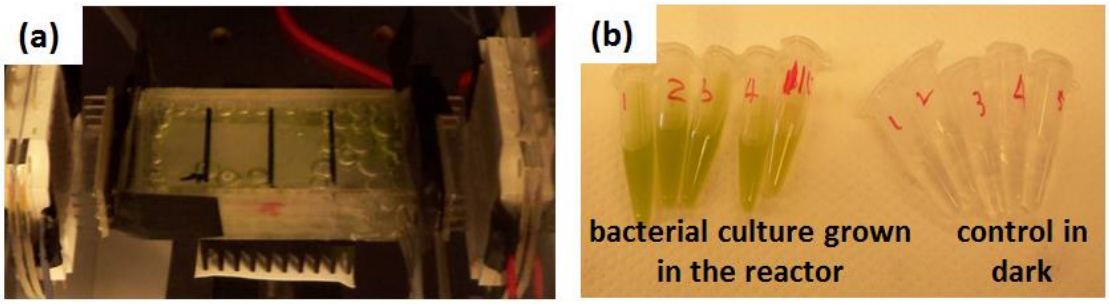

	day1	day2	day3	day4	day5
dark control	~ 0 ppm	~ 0 ppm	~ 0 ppm	~ 0 ppm	~ 0 ppm
photobioreactor	1414 ppm	1368 ppm	1755 ppm	1448 ppm	1481 ppm

Figure 5.5 Fuel production in the 10 stack photobioreactor. (a) photobioreactor with bubbles generated inside after 5 days of light illumination via LEDs (b) bacterial solution extracted from the activated (left) and non-activated (right) photobioreactors

5.4 Conclusions

In this work, we have demonstrated a bench scale 10 stack photobioreactor that utilizes the evanescent field and scattering lights of slab waveguides to culture photosynthetic organisms. The waveguide layout allowed us to minimize the shading effect that causes poor volumetric productivities in current photobioreactors. More importantly, for the first time we demonstrated the fuel production using the photobioreactor. The bench scale photobioreactor demonstrated here can provide an appropriate architecture for a new type of biofuel production reactor that utilizes the genetically modified photosynthetic organisms to produce fuel directly.

REFERENCES

1. Chisti, Y., *Biodiesel from microalgae.* Biotechnology Advances, 2007. **25**(3): p. 294-306.
2. Chisti, Y., *Biodiesel from microalgae beats bioethanol.* Trends in Biotechnology, 2008. **26**(3): p. 126-131.
3. Grima, E.M., et al., *Recovery of microalgal biomass and metabolites: process options and economics.* Biotechnology Advances, 2003. **20**(7-8): p. 491-515.
4. Torkamani, S., et al., *Plasmon-enhanced microalgal growth in miniphotobioreactors.* Applied Physics Letters, 2010. **97**(4).
5. Atsumi, S., W. Higashide, and J.C. Liao, *Direct photosynthetic recycling of carbon dioxide to isobutyraldehyde.* Nature Biotechnology, 2009. **27**(12): p. 1177-U142.
6. Atsumi, S., T. Hanai, and J.C. Liao, *Non-fermentative pathways for synthesis of branched-chain higher alcohols as biofuels.* Nature, 2008. **451**(7174): p. 86-U13.
7. Ungerer, J., et al., *Sustained photosynthetic conversion of CO2 to ethylene in recombinant cyanobacterium Synechocystis 6803.* Energy & Environmental Science, 2012. **5**(10): p. 8998-9006.

CHAPTER 6

CONCLUSIONS

In this dissertation, I presented a numerical and experimental demonstration of optofluidic reconfigurable photonic systems and novel optofluidic photobioreactors for algae based biofuel production.

6.1 Summary of accomplishments and Future directions

6.1.1 Analysis of liquid-to-solid coupling and other performance parameters for microfluidically reconfigurable photonic systems

In this chapter we demonstrated that (1) liquid waveguide's properties changed dramatically as a function of Peclet numbers and downstream distance due to diffusion of the liquid core, (2) that bending losses in liquid waveguide systems reduced by increasing the waveguide Peclet number, (3) that the evanescent coupling from the liquid to the solid waveguide is irreversible due to the diffusion of the liquid waveguide, (4) that the high coupling efficiency of fluid end-fire coupling can be obtained when the tunable MFD of the liquid waveguide was matched to that of the solid waveguide.

The numerical results obtained here provide valuable design data for the creation of several fluid-solid-optic components. For example, flexible optical switches, couplers, and splitters can be created by the evanescent coupling and end fire coupling between

the liquid and solid waveguide. The numerical results also suggest that those switches, couplers and splitters are possibly achieved by a single reconfigurable structure. The hybrid reconfigurable system allows us to save our efforts and time to design various components and to build ultracompact chips. Although I only demonstrated the combination of a simple liquid and a solid waveguide, the combination with complex components would enhance the applicability of optofluidic field in multiple scenarios. One example is the integration of the liquid waveguide and solid ring resonators. The coupling efficiency of ring resonators highly depends on the distance between the input waveguide and ring resonators. However, achieving the optimal distance for the highest coupling efficiency requires a number of trails due to fabrication errors. Therefore the flexibility of the liquid waveguide could allow ring resonators to achieve higher coupling efficiencies. Another possibility is the combination of more than one liquid and solid waveguides in a system. Studying the interaction between multiple liquid and solid waveguides will open opportunities to design robust multiple output optical switching system.

6.1.2 Continuous operation of a hybrid solid-liquid state reconfigurable photonic system without resupply of liquids

In this chapter we demonstrated the direct evanescent and end-fire coupling between liquid- and solid-state waveguides and an on-chip fluid core/cladding separation. We developed a recirculation system that reduces the consumption of liquids more than 200 fold over the state of the art and demonstrated the continuous operation of the

system for over 20hrs without performance degradation or requiring the replenishment of liquids. In this work, we have taken an important step towards the development of practical reconfigurable photonic systems.

While the fastest switching speed of the microfluidic reconfiguration demonstrated here was 0.5s, the speed can be improved by using fluids with lower viscosities and creative design of microfluidic channels, for example, using sheath flows that can deform liquid waveguides more quickly. Another possible way to improve the performance of the system would be focusing light in a 3 dimensional liquid waveguide. In the 3D liquid waveguide that focuses light in Z direction as well as X-Y directions that we demonstrated in the study, light will be more tightly confined and the reconfiguration of the liquid waveguide can be more sophisticated.

To be used as a flexible optical switch, switching light between multiple solid waveguides should be demonstrated. Although the demonstrated platform had only two output solid waveguides, array of output waveguides can be easily achieved using the fabrication technique developed in the study. In those cases, bending losses that have been analyzed in the chapter 2 would be an important parameter to optimize the system.

6.1.3 Slab waveguide photobioreactors for microalgae based biofuel production

In this chapter, I have characterized organism growth rates in novel optofluidic photobioreactors that can help address the light distribution challenge while being compatible with these chemical secreting organisms. The photon usage efficiency of

evanescent field illumination was comparable to the direct illumination used in traditional photobioreactors. I also demonstrated 12 fold improvements in volumetric productivity due to the stackable nature of the slab waveguide approach. The optofluidic approach demonstrated here can provide an appropriate architecture for a new type of biofuel production reactor that utilizes the genetically modified photosynthetic organisms to produce fuel directly. These proof of concept experiments offered useful parameters to build bench scale photobioreactors.

We can utilize the single layer photobioreactor to further optimize the light delivery and characterize the optical surface. For example, we could use line output lasers or collimated light sources to achieve the even distribution of light across the surface of the planar waveguide. Point laser that I used in the study also can achieve a uniform distribution of light using an optical cavity design (*i.e.* covering sides of the waveguide with silver to make mirror-like surfaces on which lights reflect back).

6.1.4 Stackable ultracompact photobioreactors for microalgae based biofuel production

In this chapter, I have demonstrated bench scale 10 stack photobioreactors, and characterized the growth rate of fuel producing organisms in the reactor. For the first time, I have demonstrated the fuel production from organisms grown in the 10 stack photobioreactor. The bench scale prototype demonstrated here shows the possibility to scale up stackable photobioreactors to pilot scale reactors. Design parameters utilized to build the prototype in the study can be applied to pilot scale reactors. To

successfully scale up the demonstrated prototype to a pilot scale, two improvements should be made to the existing reactor system. For the first improvement, the optical coupling of incoming light into waveguides can be improved. In the study, incoming light was coupled into the waveguide directly without any lens to focus the light and therefore the coupling efficiency was low. To improve the coupling efficiency, cylindrical lenses can be integrated with waveguides to concentrate the incoming light. The second improvement will be to enhance nutrient/carbon source delivery to the culture using a continuous controlled diffusion method. Integration of slab waveguides with hollow fibers that deliver CO_2 to photosynthetic bacteria, and remove O_2 and fuels produced by the bacteria will enhance the nutrient/carbon source delivery in the system.

6.2. Concluding Remarks

This dissertation has shown new directions in optofluidics that allow us to overcome challenges in two fields: reconfigurable photonics and photobioreactors for algae based biofuel production. In the first part of this dissertation, I have numerically and experimentally demonstrated how liquid state optical elements can be integrated with conventional solid state optical elements to create reconfigurable photonic system. In the second part of this dissertation, I have developed novel optofluidic photobioreactors that highly improve the volume productivity for the algae biofuel production. In conclusion, I have demonstrated that the fusion of optics and fluidics offers unique solutions to problems in multidisciplinary areas and will further provide

avenues where optofluidic approaches can be beneficial to address challenging problems.